Stromule extension along microtubules coordinated with actin-mediated anchoring guides perinuclear chloroplast movement during innate immunity

Amutha Sampath Kumar[1,*], Eunsook Park[2,*, §], Alexander Nedo[1,3], Ali Alqarni[1,3,4], Li Ren[4], Kyle Hoban[1,3], Shannon Modla[1], John H. McDonald[3], Chandra Kambhamettu[4], Savithramma P. Dinesh-Kumar[2,**] and Jeffrey L. Caplan[1,3,4**]

[1]Delaware Biotechnology Institute, University of Delaware, Newark, DE 19711.

[2]Department of Plant and The Genome Center, College of Biological Sciences, University of California, Davis, CA 95616.

[3]Department of Biological Sciences, College of Arts and Sciences, University of Delaware, Newark, DE 19711.

[4]Department of Plant and Soil Sciences, College of Agriculture and Natural Resources, University of Delaware, Newark, DE 19711.

[5]Department of Computer and Information Sciences, College of Engineering, University of Delaware, Newark, DE 19711.

[§] Current address: Department of Plant Sciences, College of Agriculture and Life Sciences, Seoul National University, Seoul, Korea

*Authors contributed equally to this paper

**Correspondence to:

jcaplan@udel.edu (Phone: 302-831-3403; Fax: 302-831-4841)

spdineshkumar@ucdavis.edu (Phone: 530-752-2205; Fax: 530-752-5410)

Abstract

Dynamic tubular extensions from chloroplasts called stromules have recently been shown to connect with nuclei and function during innate immunity. We demonstrate that stromules extend along microtubules (MTs) and MT organization directly affects stromule dynamics since stabilization of MTs chemically or genetically increases stromule numbers and length. Although actin filaments (AFs) are not required for stromule extension, they provide anchor points for stromules. Interestingly, there is a strong correlation between the direction of stromules from chloroplasts and the direction of chloroplast movement. Stromule-directed chloroplast movement was observed in steady-state conditions without immune induction, suggesting it is a general function of stromules in epidermal cells. Our results show that MTs and AFs may facilitate perinuclear clustering of chloroplasts during an innate immune response. We propose a model in which stromules extend along MTs and connect to AF anchor points surrounding nuclei, facilitating stromule-directed movement of chloroplasts to nuclei during innate immunity.

Introduction

Stroma-filled tubular structures called stromules emanate from chloroplasts and have been observed in several genera in the plant kingdom, although they are most common in non-green plastids (Gray et al., 2001; Hanson and Sattarzadeh, 2008; Kohler and Hanson, 2000; Kumar et al., 2014; Natesan et al., 2005). Stromules are developmentally regulated and induced in response to biotic and abiotic stress, symbiotic association, and changes in plastid number and size (Brunkard et al., 2015; Caplan et al., 2015; Caplan et al., 2008; Erickson et al., 2014; Gray et al., 2012; Kumar et al., 2014; Schattat and Klosgen, 2011; Waters et al., 2004). The dynamic extension of stromules increases the surface area of chloroplasts, presumably facilitating transport of signals or macromolecules to the nucleus, cytosol, plasma membrane or other organelles (Gunning, 2005; Kwok and Hanson, 2004a; Kwok and Hanson, 2004c). We have recently shown that stromules are induced and function during innate immunity (Caplan et al., 2015). The induced stromules make connections with the nuclei to facilitate transport of chloroplast-localized defense protein NRIP1 (N receptor interacting protein 1) and the pro-defense molecule, hydrogen peroxide (H_2O_2), from chloroplasts into nuclei during an immune response (Caplan et al., 2015). Stromules may also facilitate certain number of chloroplasts to maintain contact with the moving nuclei (Erickson et al., 2017a). However, the mechanism(s) that facilitates chloroplast stromules connections to nuclei and eventual perinuclear clustering of chloroplasts is unknown.

Stromule length is variable as they extend, retract and branch, changing their shape and position (Gray et al., 2001; Gunning, 2005; Kwok and Hanson, 2004c; Waters et al., 2004). However, mechanisms that regulate the dynamic nature of stromule morphology and motility are poorly understood. Studies using inhibitors in non-green tissue have implicated cytoskeleton

elements such as actin microfilaments (AFs) and microtubules (MTs) in regulating stromule frequency, length and motility (Gunning, 2005; Kwok and Hanson, 2003; Kwok and Hanson, 2004a). Treatment with AF inhibitors, Cytochalasin D (CTD) and Latrunculin B, resulted in the reduction of stromule frequency in tobacco hypocotyls (Kwok and Hanson, 2003). Stromules have been observed to extend parallel to AFs and the tips of stromules make contact with AFs in Arabidopsis hypocotyl epidermal cells (Kwok and Hanson, 2004a). Treatment with myosin ATPase inhibitor 2,3 butanedione 2-monoxime (BDM) affects stromule movement and length; furthermore, Myosin XI family motor proteins have been implicated in stromule movement and anchoring to the cytoskeleton in *Nicotiana* (Natesan et al., 2009; Sattarzadeh et al., 2009). These findings suggest that stromules move along AFs using myosin motors; however, direct evidence for movement along AFs is lacking. Treatment with MT inhibitor amiprophosmethyl (APM) reduced stromules, and co-treatment with AF and MT inhibitors decreased stromule frequency and length (Kwok and Hanson, 2003). In contrast, "chloroplast protrusions" from mesophyll chloroplasts of the arctic plant *Oxyria digyna* remained unaffected by the MT inhibitor Oryzalin or the AF inhibitor LatB (Holzinger et al., 2007b). Therefore, the precise role of AFs and MTs during stromule dynamics in green tissue chloroplasts is not well understood.

Here, we analyzed the mechanism of stromule extension and movement in chloroplasts of green leaf tissue and perinuclear chloroplast clustering during innate immunity. Our results show that MTs are required for stromule extension and movement. MT depolymerization led to stromule retraction, and MT stabilization increased stromule frequency. Silencing the gene for γ-tubulin complex protein 4 (GCP4) caused enhanced bundling and disrupted dynamics of MTs, which resulted in longer stromules, but slower extension and retraction. Although stromule extension does not require AFs, they function as anchor points that stabilize stromules and

anchor the body of chloroplasts. AFs play an important role in type of chloroplast movement that appears to be directed by stromules. This new type of stromule-directed movement is completely disrupted by AF inhibitors. However, stromule-directed chloroplast movement was still observed when AFs were partially disrupted, suggesting that chloroplast anchoring might restrict stromule directed movement. We hypothesize that a biological function of stromules is to direct the movement of chloroplasts. During an innate immune response, we propose a model where stromules extend along MTs towards nuclei and attach to the nuclei at actin anchor points; and, these perinuclear stromule attachments guide chloroplasts to the nucleus.

Results

Stromules interact and extend along microtubules

To examine the interactions of stromules with MTs, we expressed TagRFP fused to the N-terminal microtubule associated protein domain of CKL6 (Ben-Nissan et al., 2008) (TagRFP-MAP-CKL6) in transgenic *Nicotiana benthamiana* plants expressing NRIP1 fused to Cerulean (NRIP1-Cerulean) that mark stromules (Caplan et al., 2015; Caplan et al., 2008). Marking both stromules and MTs revealed that these two structures overlapped in confocal microscopy images. These sites of overlap were designated as potential stromule-to-MT interactions. These observations were made in maximum intensity projections of z-stacks generated by confocal microscopy, and all observations in this study, were made in epidermal pavement cells of *N. benthamiana* plants. The varied morphology of stromules appeared to be correlated with MT interactions (*Figure 1*). Stromules often initiate as beak-like structures. The tips of beaks were seen interacting with MTs (*Figure 1A*; column 1). Beaks extend into longer stromules. Longer

stromules were seen as just the tips of stromules interacting with MTs or the tip and the full length of the stromule aligned with MTs (*Figure 1A*; column 2 and 3). More complex stromule structures, such as kinked or branched stromules, were found at the junction of two MTs (*Figure 1A*; column 4 and 5). However, approximately 11% of stromules did not interact with MTs (*Figure 1A*, arrowhead), suggesting there is a MT-independent mechanism of stromule formation.

A stromule-to-MT interaction was designated if these two structures were overlapping or not resolvable by confocal microscopy. However, since the resolution of confocal microscopy is relatively low, we verified the close interaction between stromules and MTs using transmission electron microscopy (TEM). Microtubules were originally detected and described in plants using TEM and can readily be observed as hollow, tubule-like structures that are 24 nm in diameter (Ledbetter and Porter, 1963). We were able to observe MTs by TEM and the close interactions of MTs with stromule tips and kink points (*Figure 1-figure supplement 1*). MTs were seen directly associated with the chloroplast outer envelope membrane at a kink point. Serial sections near the tip of a stromule that graze the chloroplast outer envelope membrane show MTs in line and in close proximity to the stromule.

Since our initial observations were from static images of stromules interacting with MTs, to look at the dynamics of stromules along MTs, we used an established transgenic *N. benthamiana* MT marker line expressing green fluorescent protein fused with the tubulin alpha 6 (GFP-TUA6) (Gillespie et al., 2002). In this transgenic line, we expressed NRIP1's chloroplast transit peptide fused to TagRFP [NRIP1(cTP)-TagRFP] to mark stromules (Caplan et al., 2015). Time-lapse imaging of GFP-TUA6 labeled MTs revealed that stromules dynamically extended along MTs (*Figure 1B*, Video 1). Kymographs of the motion showed stromules extending and retracting in

line with MTs in a single direction (*Figure 1B*, left kymograph) or moving bi-directionally in opposite directions (*Figure 1B*, bottom right kymograph). We also verified the stromule movement using another MT marker, the end binding 1 protein (Chan et al., 2003) fused to Citrine (EB1-Citrine). EB1-Citrine was initially chosen to examine the direction of movement because EB1 marks the positive end of MTs; however, the *Agrobacterium*-mediated expression often led to even staining of the MTs (*Figure 1C*). Kymographs of the motion of stromules showed clear movement of stromule tips along MTs (*Figure 1C*). The time lapse video show the dynamic interactions of stromules with MT, including branching, tip contact, transfer between microtubules, stromule initiation and bidirectional extension (Video 2). Our results from using three different MT markers via transgenic and transient expression indicate that stromules extend along MTs.

To quantify the motion, we manually tracked the velocity of stromules extending along MTs. All stromule extension was correlated with movement along MTs. The velocity of stromule extension was significantly lower when MTs were marked with EB1-Citrine (0.0565 μm/s) compared to GFP-TUA6 (0.146 μm/s) (*Figure 1D*). An automated algorithm for detecting stromule tips in maximum intensity projections was developed (Lu et al., 2017). The MTs were segmented and skeletonized (data not shown). Using the skeletonized images, the points of interaction (*Figure 1E*, green) and the points of no interaction (*Figure 1E*, red) were mapped over a time series (Video 2). Linear arrays of interaction points along MTs were clearly seen in time points T= 6, 12, and 18 min (*Figure 1E*). A retraction event had limited interaction with MTs (*Figure 1E*, arrowhead). The algorithm only accurately detected the slower moving motion when EB1-Citrine was used as a MT marker, and therefore, was not used in other experiments.

The length, velocities, extension and retraction frequencies, and types of motion were quantified manually in all other experiments.

Stromule extensions through the ER is directed by microtubules

Stromules and the endoplasmic reticulum (ER) have correlated dynamics and three-dimensional arrangement; therefore, it was hypothesized that contact points along the ER direct their extension (Schattat et al., 2011). Since, our data suggested that the extension of stromules is directed by MTs, we examined stromules, ER and MTs simultaneously by co-expression of labels for the ER (SP-Citrine-HDEL) and MTs (TagRFP-MAP-CKL6) in NRIP1-Cerulean transgenic *N. benthamiana* plants that mark stromules. Similar to the previous report (Schattat et al., 2011), stromules were surrounded by ER, but here we show that MTs direct the movement through ER (*Figure 2A*; Video 3). Imaging using a high-resolution airyscan confocal microscope revealed that the ER forms channels around the stromules, and MTs were found at the stromule-to-ER interface (*Figure 2B*). Time lapse studies under similar imaging conditions showed that stromule extension occurred actively along the MTs while the ER changed its direction and formed a channel around the extended stromule tip (*Figure 2C*, middle panel; Video 4). The stromule continued to extend along the MTs past the ER and no longer formed a channel around the extending stromule tip (*Figure 2C*, right panel). These time-lapse studies indicate that stromule extension is active along MTs and ER reorganization follows stromule extension along MTs.

184 **Microtubules are required for stromule formation and extension**

185 To further demonstrate that stromules extend along MTs, we expressed the MT marker
186 TagRFP-MAP-CKL6 in NRIP1-Cerulean transgenic *N. benthamiana* plants and then disrupted
187 MTs using 20 μM APM or 300 μM Oryzalin. Compared to the DMSO vehicle control (*Figure*
188 *3A*, top panel), depolymerization of MTs was noticeable 5 to 15 min after APM and Oryzalin
189 treatment, leaving behind remnants of partially depolymerized MTs and an increase of the MAP-
190 CKL6 MT marker in the cytosol (*Figure 3A*, middle and bottom panels). Although mock control
191 with DMSO resulted in an increase in stromules compared to the infiltration media control, the
192 APM or Oryzalin disruption of MTs for 15 min significantly inhibited this increase in stromule
193 number (*Figure 3B*). MT depolymerizers APM and Oryzalin not only decreased stromule
194 number but also restricted stromules to MT fragments causing changes in stromule movement
195 (Video 5). Beak-like protrusions from chloroplasts that did not result in stromules were also
196 observed in APM and Oryzalin treatment (*Figure 3A*, asterisk; Video 5), however, we did not
197 determine if these increased with the treatments compared to the DMSO vehicle control. In the
198 time-lapsed data set shown in Figure 3A, stromule length was gradually reduced during 15 min
199 treatment with APM that was caused by stromule retraction and correlated with simultaneous
200 depolymerization of the MTs and, eventually, complete retraction of stromules (*Figure 3A*,
201 middle and bottom panels, arrowhead). Similarly, with Oryzalin treatment at 0 min, we observed
202 a region of the stromule overlapped with a segment of the MT (*Figure 3A*, bottom panel, T=0).
203 As the time course progressed, the segment of MT became shorter and there was a corresponding
204 reduction in the length of the stromule (*Figure 3A*, bottom panels). In that time-lapsed data set, at
205 15 min treatment with Oryzalin we observed that stromules completely retracted from and
206 changed course from the MT (*Figure 3A*, bottom panel, T=15; Video 5). These results indicate

that the disappearance of stromules may be a combination of disruption of extended stromules and the prevention of induction of new stromules.

Changes in microtubule organization increases stromule number, length and stability

Since our results from MT inhibitor studies indicated that stromule formation and extension require MTs, we tested the effect of stabilizing MTs using Taxol (Schiff and Horwitz, 1980). Infiltration of Paclitaxel-BODIPY conjugate into leaves of transgenic NRIP1-Cerulean *N. benthamiana* plants showed extensive MT stabilization after 30 min of treatment compared to the mock control (*Figure 3C*) and significantly induced stromules compared to mock control (*Figure 3C-D*). Interestingly, after Paclitaxel treatment, we observed long stromules and multiple stromules emanating from individual chloroplasts (*Figure 3C*, bottom panels). These results suggest that MT stabilization is sufficient to induce stromules.

To more specifically alter MT organization and dynamics, we knocked-down the expression of *GCP4* in *N. benthamiana* plants using virus-induced gene silencing (VIGS) approach (Dinesh-Kumar et al., 2003). GCP4 is a subunit of the γ-tubulin complex and artificial miRNA (amiR)-mediated knockdown of Arabidopsis *GCP4* resulted in hyper-parallel and bundled cortical MT in leaf epidermal cells (Kong et al., 2010). We silenced *NbGCP4* in NRIP1-Cerulean and GFP-TUA6 transgenic *N. benthamiana* plants to visualize the effect on stromules and MTs respectively. Since *amiR-AtGCP4* in *Arabidopsis* plants resulted in a significant growth phenotype, we first determined how many days of *NbGCP4* VIGS resulted in a MT alteration without a severe growth phenotype. Four days after silencing, *NbGCP4*-silenced plants phenotypically looked similar to that of VIGS vector control plants (*Figure 4-figure supplement 1A*). However, six days post-silencing, leaves of the *NbGCP4*-silenced plants developed a

crinkled leaf phenotype (*Figure 4-figure supplement 1B*, right panel). In addition, at this time point the NRIP1-Cerulean stromule marker begin to leak out of chloroplasts compared to the VIGS control plants (*Figure 4-supplement figure 1C*, right panel). Fourteen days post-silencing, *NbGCP4*-silenced plants showed severe growth arrest and morphological distortion (*Figure 4-figure supplement 1D*). Thus, we observed stromules in leaf epidermal cells of the plants after four days of *NbGCP4* VIGS, to minimize potential physiological changes that might occur due to the alterations of MT organization and dynamics. Although at four days-post silencing, *NbGCP4* mRNA levels are reduced by only 50% in the silenced plants compared to the VIGS control plants (*Figure 4B*), cortical MT organization was significantly altered in the leaves of *NbGCP4*-silenced plants compared to the control (*Figure 4A*) in a similar way to *amiR-AtGCP4* in *Arabidopsis* (Kong et al., 2010). To quantify these changes, we used SOAX software that uses Stretching Open Active Contours (SOACs) to quantify filamentous networks (Xu et al., 2015). SOAX analysis showed that MTs were more parallel or aligned in *NbGCP4*-silenced plants compared to the vector control (*Figure 4C*), which was visible by displaying the MT direction by color-coding the azimuthal angles (*Figure 4D*). Quantitative SOAX analysis shows that silencing *NbGCP4* decreases the curvature (*Figure 4E*) and increases the snake length fitted to MTs (*Figure 4F*). The snake length is not a direct measurement of MT length, since this approach cannot accurately distinguish between two MTs that are bundled together. Nonetheless, this measurement further suggests that silencing *NbGCP4* alters MTs.

The alteration in MT organization at four days-post silencing of *NbGCP4* (*Figure 4*), resulted in more than twice the number of stromules in *NbGCP4*-silenced plants compared to the VIGS vector control (*Figure 5A*, top panels; 5B, compare bars in mock treatment). Stromules were on average significantly longer in *NbGCP4*-silenced plants compared to VIGS vector control

253 (*Figure 5A*, top panels; *Figure 5C*, compare bars in mock treatment). Furthermore, a greater
254 percentage of stromules were longer than 3 μm in *NbGCP4*-silenced plants (*Figure 5- figure*
255 *supplement* 1A). We classified stromule movement into three types, smooth and constant
256 movement, sudden and erratic movement, and side and tangential movement (*Figure 5-figure*
257 *supplement* 1B) and found that, in *NbGCP4*-silenced plants, stromule movements were more
258 constant than those in VIGS vector control (*Figure 5-figure supplement* 1C).

259 We recently reported that stromules are induced significantly during an immune response
260 against bacterial and viral infections (Caplan et al., 2015). The nucleotide-binding domain
261 leucine-rich repeat (NLR) immune receptor N recognizes p50 effector from Tobacco Mosaic
262 Virus (TMV) and activate immune response to limit TMV to the infection site (Whitham et al.,
263 1994). The stromules are significantly induced during N NLR-mediated immunity to TMV
264 (Caplan et al., 2015). Therefore, we tested if N NLR-mediated activation of immune response
265 could further increase stromule number and length in *NbGCP4*-silenced plants. For this, we
266 silenced *NbGCP4* in transgenic *N. benthamiana* expressing N NLR and NRIP1-Cerulean
267 (stromule marker) for three days and then infiltrated with p50 and 24 hours later the observations
268 were recorded. As shown before (Caplan et al., 2015), the number of stromules significantly
269 increased in p50-treated VIGS vector control plants compared to mock-treatment (*Figure 5A*,
270 compare left panels and 5B, compare green bars). The average length (*Figure 5C,* green bars)
271 and percentage of stromules longer than 3 μm also increased during an immune response (*Figure*
272 *5-figure supplement* 1A). Interestingly, the increase in stromules in mock-treated *NbGCP4*-
273 silenced plants and a p50-induced immune response in VIGS vector control were remarkably
274 similar (*Figure 5A*, compare top right panel with bottom left panel; *Figure 5B*, compare mock-
275 treated magenta bar with p50-treated green bar). There was no significant change in stromule

number in p50-treated *NbGCP4*-silenced plants compared to the mock-treated *NbGCP4*-silenced plants (*Figure 5A*, right panels and 5B, compare magenta bars). Mock-treated *NbGCP4*-silenced plants also showed longer stromules compared to mock-treated VIGS vector control plants (*Figure 5C*). This increase was similar to that of in p50-treated VIGS vector control plants that showed significantly longer stromules compared to mock-treated plants (*Figure 5C*, compare green open bars). However, there was no significant difference in stromule length in p50- and mock-treated *NbGCP4*-silenced plants (*Figure 5C*, compare magenta open bars). Collectively, these results indicate that the activation of immune response does not further increase stromule number and length in *NbGCP4*-silenced plants that exhibit constitutive stromule induction.

The velocities of stromule extension and retraction were calculated as an indicator of stromule dynamicity and stability. The stromule extension and retraction velocities decreased in the *NbGCP4*-silenced plants compared to the VIGS vector control (*Figure 5D*), suggesting that stromules were less dynamic and more stable. These results indicate that specific alterations of MTs are correlated with change in stromule dynamics and further support a role for MTs in regulating stromules. Interestingly, p50-treated VIGS vector control compared to the mock treatment reduced the velocities of stromule extension and retraction (*Figure 5D*, compare green bars) suggesting that stromules are less dynamic and more stable during active immune response. To test if p50-induced immunity alters MT organization resulting in alteration in stromule dynamics, we observed MT dynamics upon TMV-p50 treatment. For this, MT marker TagRFP-MAP-CKL6 was infiltrated into transgenic *N. benthamiana* plants expressing N NLR and NRIP1-Cerulean (*NN*) or expressing only NRIP1-Celulean without N NLR (*nn*). 12 hours later, p50 was infiltrated into the same spot to induce an immune response. After 48 hours of TagRFP-MAP-CKL6 expression and 36 hours of p50 expression, the MT cytoskeleton was imaged and

299 then analyzed by SOAX. Visible differences in MTs between immunity-induced plants (*Figure*
300 *5E*, *NN*+p50) and non-immunity induced plants (Figure 5E, *nn*+p50) were difficult to observed
301 in the images, but interestingly, SOAX analysis revealed that p50 induced immunity altered MT
302 morphology (*Figure 5F-H*). Specifically, there were minor differences in orientation (*Figure*
303 *5F*), curvatures were significantly smaller (Figure 5G) and snake lengths were larger (*Figure 5H*)
304 in *NN*+p50 compared to *nn*+p50. Collectively, these results indicate that changes in MT
305 organization caused by *NbGCP4*-silencing plants or during p50-induced immunity are correlated
306 with changes in stromule dynamics, indicating a possible direct or indirect role for MT
307 organization in modulating stromule dynamics.
308
309 **Actin filaments serve as anchor points but not as tracks for stromule extension**
310 Since AFs were previously shown to regulate chloroplast movement and stromule
311 morphology (Kwok and Hanson, 2003; Kwok and Hanson, 2004a), we tested if stromules extend
312 along AFs. We expressed Lifeact-TagRFP that labels AF (Era et al., 2009; Riedl et al., 2008) in
313 transgenic *N. benthamiana* plants expressing NRIP1-Cerulean that marks stromules (Caplan et
314 al., 2015; Caplan et al., 2008). Out of 73 stromule tip extension events from 34 cells, the vast
315 majority (93%) of stromule tip extensions were not observed along AFs. Stromules were
316 occasionally observed to be aligned with AF (*Figure 6A*, asterisk), but high-resolution
317 examination showed that they were not co-localizing (*Figure 6-figure supplement 1*). Instead, in
318 many cases, stromules interacted at restricted foci (*Figure 6A*, arrowheads) that often
319 corresponded with a kink in the stromule. We verified these interactions using TEM and found
320 an AF bundle in close proximity to the apex of a stromule kink (*Figure 6-figure supplement 2A-*

B). Stromule tips often reached actin filaments (*Figure 6A*, arrows), however, time-lapse videos showed stromules interacting with AFs, but not extending along AFs (Video 6).

To determine if actin plays another role in stromule dynamics, we performed time-lapse studies in epidermal cells expressing the actin marker Lifeact-TagRFP. Stromules appeared to interact statically, and not dynamically, with AFs, suggesting there are actin anchor points along stromules. Interactions were observed at the tips or at kink points (*Figure 6B*). Kymographs and time lapsed video show that retracting stromules paused for multiple, consecutive time frames or stopped completely at AFs (*Figure 6C, Figure 6- figure supplement 1,* Video 7). Due to the density of the AF network, stromules are often seen intersecting with AFs. To indirectly determine if those points of intersection are potential AF anchor points, we examined stromule retraction events. 19.4% of stromules retracted fully back to the body of the chloroplast without any pausing, often passing intersections with AFs. 77.1% of retracting stromule tips paused for multiple, consecutive frames and showed colocalization with an AF. 5.7% of retracting stromule tips paused for multiple, consecutive frames, but did not colocalize with AF (*Figure 6D*). The pausing of retracting stromules at AF cannot be explained by chance alone because the density of AFs and the colocalization of stromules with AFs observed appeared to be much less than 77.1% (*Figure 6A; Figure 6 - figure supplement 1; Video 7)*. Therefore, this data suggests that there are actin anchor points along stromules. We further examined the interaction of stromules and AFs by expressing mTalin-Citrine in NRIP1-Cerulean *N. benthamiana* plants and then examining by high-resolution airyscan confocal microscopy (*Figure 6E*). AF marker mTalin-Citrine has been used previously to detect chloroplast-associated actin (cp-actin) (Kadota et al., 2009). We could observe clear interactions of AF with chloroplast bodies (*Figure 6E*). Interestingly, we observed a clear thinning or constriction at the site of stromule-to-actin interaction points along the length

and across the body of the chloroplast (*Figure 6E*; arrowheads). Three-dimensional modeling shows grooves across the body of the chloroplast that correlate with AFs (*Figure 6E, Figure 6-figure supplement 2C-D*). Although, the mechanism of stromule thinning at actin interaction sites is unknown, collectively these results indicate that AFs provide anchor points for stromules but not tracks for stromule extension.

To determine the effect of AF disruption on stromule formation, we expressed mTalin-Citrine in NRIP1-Cerulean transgenic lines and applied 200 μM Cytochalasin D (CTD) to depolymerize AFs for 30 min (*Figure 6-figure supplement 3*). Since CTD treatment disrupted the actin network only in a fraction of the cells, only cells with a disrupted actin network were examined. Stromules were still present in cells where actin network was disrupted (*Figure 6-figure supplement 3A*) and the stromule number was similar between the CTD- and mock-treatments (*Figure 6-figure supplement 3B*).

Microtubules and actin filaments contribute to stromule dynamics

Several studies suggested that MT and AF networks might work cooperatively for maintaining cell structure and physiology in eukaryotic systems (reviewed in (Takeuchi et al., 2017)). Although stromule formation and extension is primarily associated with MTs, AFs might have a role in stromule dynamics. To examine the role of each cytoskeletal filament, we treated transgenic *N. benthamiana* plants expressing GFP-TUA6 that marks MTs and FABD2-GFP that marks AFs with longer treatments of low concentrations of cytoskeleton inhibitors that specifically disrupt one cytoskeleton component, but not other. These experiments are in contrast to shorter treatments of higher concentrations (*Figure 3, Figure 6-figure supplement 3*) that are not optimal for time lapsed acquisition of stromule dynamics. We found that treatment with 1

μM of oryzalin (ORY) treatment for 1 hour partially disrupted MTs and had no significant, visible effect on the AF network (*Figure 7-figure supplement 1*, middle panels). Next, we tested CTD treatment concentrations to disrupt AFs. 10 μM of CTD treatment for 1 hour fully disrupted actin filament AF network showing bright puncta of GFP-FABD2, but only had a mild effect on MT organization (*Figure 7-figure supplement 1*, right panels); therefore, we used 10 μM of CTD. NRIP1-Cerulean transgenic plants were treated with either 10 μM CTD or 1 μM ORY for 1 hour to disrupt AFs or MTs respectively, and then stromule length and dynamics were analyzed (*Figure 7A*). Interestingly, although average stromule length in both drug treatments were not significantly different (*Figure 7B*), velocity of stromule extension was increased significantly in ORY treatment compared to DMSO control (*Figure 7C*). Furthermore, CTD treatment resulted in significant reduction in velocity of both stromule extension and retraction compared to the control (*Figure 7C*). Interestingly, CTD treatment increased constant and smooth movements of stromules and reduced sudden and erratic movements of stromules, suggesting that CTD treatment stabilizes stromule dynamics (*Figure 7D*). Together, these results indicate that both types of cytoskeletal filaments regulate stromule dynamics.

Stromules direct chloroplast movement

While analyzing time-lapsed images of stromule movements in *N. benthamiana* transgenic plants expressing NRIP1-Cerulean, we observed the movement of chloroplasts in the direction of stromules (*Figure 8A; Video 8*) or towards stromule kinks that are correlated with anchor points (*Figure 6, Figure 8-figure supplement 1*). This observation suggests that stromules might direct or guide chloroplast movement. To examine if this movement is correlated with the interactions with the cytoskeleton, we co-expressed Lifeact-TagRFP that marks AFs and NRIP1(cTP)-

TagBFP that marks stromules in *N. benthamiana* transgenic plants expressing GFP-TUA6 that marks MTs (*Figure 8B*). Stromules were anchored to AF and connected to MT for extension at 0 min. Stromules extend along MT at 1 min and retracted to the actin anchor point at 3 min. Stromule reextend on MT at 8 min. Retraction of stromule at 9 min led to movement of chloroplast body toward the direction of the stromule movement (*Figure 8B; Video 9*).

Next, we investigated if the stromule angle and the angle of chloroplast movement are significantly correlated and changed by ORY or CTD treatment. Since CTD treatment resulted in a complete disruption of chloroplast movement (*Video 10*), it was not analyzed. Chloroplast movement was first identified as any movement larger than the radius of the chloroplast body and the direction of the movement was measured as the angle from the start and end points of each movement events. If a chloroplast changed direction, that was considered a separate movement event. Only chloroplasts containing one or more stromules were used for this analysis because it depends on comparing paired measurements of the angle of the stromule from the chloroplast body attachment point to the tip and the angle of chloroplast movement. We compared 33 pairs for DMSO control and 47 pairs for ORY to calculate a circular correlation coefficient, r(FL) (Fisher and Lee, 1983). An r(FL) value of 1.0 would indicate that the stromule angle and the angle of chloroplast movement are always identical, an r(FL) of -1.0 would mean the paired angles differ by 180 degrees, and if the angles are randomly matched the r(FL) will be close to zero. The r(FL) values for DMSO and ORY were 0.76 and 0.85, respectively. To test the statistical significance, each data set was randomly shuffled 10,000 times and the r(FL) calculated for each randomization; the observed f(FL) values were greater than all of the randomized r(FL) values, so for both DMSO and ORY the stromule angle and the angle of chloroplast movement were significantly correlated ($P<0.0001$). Standard errors of the r(FL)

values were calculated using the jackknife method (Sokal and Rohlf, 1995), and used in a two-sample t-test; the r(FL) values for DMSO and ORY were not significantly different from each other (P=0.52). We generated a scatter plot of chloroplast movement angles and stromule angles, which shows a fairly linear relationship compared to the randomized control (*Figure 8-figure supplement 1*). To further visualize these data, we calculated the difference between the two angles and plotted the frequency (*Figure 8C*). If the chloroplast movement angle and stromule angle are equal, then the difference will be zero. We observed a higher frequency around zero compared to the randomized control. An examination of only angle pairs with less than $\pm$30 degree difference were highly correlated and had an r(FL) value of 0.95; we therefore defined a stromule-directed movement event as being within $\pm$30 degrees. The circular correlation calculation requires paired stromule angles and chloroplast movement angles, and excludes chloroplasts that move but do not have stromules. Using the $\pm$30 degree criteria for stromule directed movement, we were able to compare the percent of stromule driven movement compared to total movement events, which includes chloroplasts without stromules This analysis shows that ORY treatment decreased stromule-directed chloroplast movement and CTD disrupted nearly all chloroplast movement, including stromule-directed (*Figure 8D*). It is possible that stromule extension or retraction may provide the driving force for stromule-directed movement. Therefore, we quantified how many times stromule extension and retraction events occur in 10 mins after 1 hour of drug treatment. Interestingly, ORY treatment significantly increased retractions and reduced the number of extensions (*Figure 8E*); however, the remaining stromules extension showed a higher velocity (*Figure 7C*) suggesting the frequency rather than the velocity of stromule extension is with correlated chloroplast movement. Overall, these results suggest that ORY treatment caused the reduced stromule-directed chloroplast movement due to

436 less extension events. Our data show that stromules may direct chloroplast movement in
437 epidermal pavement cells; however, it remains unknown if stromules provide a driving force or
438 only guide chloroplast movement.

439 The longer CTD treatment resulted in a complete disruption of AFs and nearly all chloroplast
440 movement. Since chloroplasts are anchored to the AF network, we aimed to partially disrupt the
441 AF network without fully abrogating all AF function. Treatment with CTD resulted in
442 discontinuous AFs (*Figure 8-figure supplement 2A*, magenta) while the MTs were intact (*Figure*
443 *8-figure supplement 2A*, yellow). Examination of time lapsed maximum intensity projections of
444 confocal micrographs showed that stromules were still present at 3 min and then briefly absent at
445 approximately 8 min after CTD treatment (*Figure 8-figure supplement 2A, Video 11*). This brief
446 disruption further supports that stromules are stabilized by AF anchors and disruption of AFs
447 results in rapid retraction of stromules. However, despite the initial disruption, stromules re-
448 extended along MTs and multiple stromules were observed after 20 min (*Figure 8-figure*
449 *supplement 2A*). These observations explain why the disruption of stromules by CTD was missed
450 during 30 min treatment (*Figure 6-figure supplement 3*). Tracking the stromule and chloroplast
451 movement (Lu et al., 2017) showed that stromules can still direct chloroplast movement if AFs
452 are only partially disrupted. One chloroplast (Cp1) had restricted movement and colocalized with
453 an AF fragment (*Figure 8-figure supplement 2A)*. Stromules were observed extending in
454 opposite directions (*Figure 8-figure supplement 2B*). However, the second chloroplast (Cp2) did
455 not co-localize with AF fragments (*Figure 8-figure supplement 2A*; Video 11). The stromule of
456 this chloroplast not only extended, but its extension along the MTs facilitated a rapid pulling of
457 the body of down the viewing plane (*Figure 8-figure supplement 2C*).
458

Actin microfilaments mediate perinuclear chloroplast clustering during plant immune response

Our previous findings indicate that N NLR immune receptor-triggered immunity to the TMV p50 effector resulted in stromule induction, stromule-to-nuclear connections and eventual perinuclear clustering of chloroplasts (Caplan et al., 2015). Electron microscopy results in our previous studies indicated that the chloroplast and nuclear membranes do not directly interact (Caplan et al., 2015), suggesting other cytoplasmic components are required for this interaction. To study the importance of cytoskeleton during the process of perinuclear chloroplast clustering, we expressed TMV-p50 to induce an immune response in N-containing NRIP1-Cerulean *N. benthamiana* transgenic plants (Caplan et al., 2015; Caplan et al., 2008). Since stromules extend along MTs, initially, we marked MTs and looked at stromules to nuclear connections, but we were unable to find significant connections of stromules to MTs around nuclei. Therefore, we next marked AFs with Lifeact-TagRFP and found connections between stromules and AFs surrounding nuclei (*Figure 9*). Time-lapse studies showed long stromules stably connecting to an AF attached to a nucleus for approximately 18 min (*Figure 9A*, arrowheads). After 18 min of continuous imaging, a long stromule retracted, bringing the chloroplast body close to the nucleus (*Figure 9A*, arrows; Video 12). We verified these results with another AF marker, mTalin-Citrine (*Figure 9-figure supplement 1*). We also observed that when the bodies of chloroplasts were in contact with nuclei, there were connections with AFs (*Figure 9B-C*, arrows).

Since p50 induced immunity leads to vigorous stromule induction (Caplan et al., 2015); *Figure 5*), we hypothesized that more chloroplasts might move toward nucleus by stromule-directed movement of chloroplast body. Therefore, we quantified the perinuclear chloroplast clustering during TMV-p50 induced immune response in N-containing NRIP1-Cerulean

transgenic plants in a time course (*Figure 10A-B*). Although majority of nuclei had a low number of interacting chloroplasts in the control (*Figure 10A*, left panels), we observed a significantly higher number of chloroplasts around nuclei in TMV-p50 treated samples (*Figure 10A*, right panels). More than 80% of nuclei (85 out of 105) were surrounded by more than 2 chloroplasts in TMV-p50 treated samples compared to 50% of observed nuclei (56 out of 120) were surrounded by none or single chloroplast in the control (*Figure 10A and Figure 10-figure supplement 1A*). The ratio of nuclei-clustered with more than 4 chloroplasts was significantly higher in TMV-p50 treatment compared to the control (*Figure 10B and Figure 10-figure supplement 1A*). These results indicate significant induction of perinuclear chloroplast clustering during an immune response.

To determine, if AF anchoring plays a role in the immunity-induced perinuclear clustering of chloroplasts, we treated plants with CTD and ORY. Remarkably, CTD treatment significantly reduced the number of chloroplasts interacting with nuclei compared to the control and ORY treatment (*Figure 10C-D and Figure 10-figure supplement 1B*). These results support that anchoring of stromules to the AFs at the nucleus or more generally chloroplast movement is important for perinuclear clustering of chloroplasts during plant immune response. In conclusion, we propose a model in which perinuclear clustering of chloroplasts involves stromule anchoring to AFs surrounding nuclei and stromules guide chloroplasts towards nuclei during an immune response.

Discussion

Cytoskeletal elements in plant cells support several cellular functions, including cytoplasmic streaming, cell division, cell elongation, polar growth, vesicle trafficking, nuclear positioning

505 and morphogenesis (Cai et al., 2015; Higa et al., 2014; Li et al., 2015). In this study, we show
506 that dynamic stromules extend along MTs and AFs stabilize stromules and chloroplast-to-nuclear
507 connections during innate immune response. Stromules have the ability to direct chloroplast
508 movement, and AF anchoring of stromules may guide perinuclear chloroplast clustering during
509 innate immunity.

510 Previous studies in non-green hypocotyls indicated a role for AFs and MTs during stromule
511 formation (Kwok and Hanson, 2003; Kwok and Hanson, 2004a). The initial study (Kwok and
512 Hanson, 2003) used cytoskeletal inhibitors to implicate AFs and MTs during stromule formation,
513 suggesting that AFs promote while MTs restrict stromule and plastid movement. Stromules
514 visualized by differential interference contrast were observed interacting directly with AFs
515 labeled with GFP-hTalin and rearrangements of the AF network changed stromule morphology
516 (Kwok and Hanson, 2004a). Movement along AFs was indirectly implicated by the identification
517 of myosin XI cargo domain and a small tail domain that localize to chloroplasts (Natesan et al.,
518 2009; Sattarzadeh et al., 2009). Knockdown of myosin XIs qualitatively disrupted stromules
519 (Sattarzadeh et al., 2009) or quantitatively decreased the percent of plastids with stromules
520 (Natesan et al., 2009). However, the dynamics of stromules moving along AFs were not
521 examined in these studies (Natesan et al., 2009; Sattarzadeh et al., 2009). Furthermore, longer
522 myosin XI tail domain (Reisen and Hanson, 2007) and full-length myosin XI (Avisar et al.,
523 2008) do not localize to the chloroplasts. These studies prompted us to conduct a detailed time-
524 lapse confocal microscopy of the dynamics of stromules and AFs. Surprisingly, our extensive
525 investigations were unable to show extension of stromules along AFs. Instead, we discovered
526 stromules were statically anchored to the AF network. Stromules were previously shown to
527 actively move beyond AF attachment points via an unknown mechanism that was proposed to be

528 either collisions with other components of the cytoplasm or interactions with very fine AFs
529 (Kwok and Hanson, 2004a). Here we have revealed that this unknown mechanism to be stromule
530 extension along MTs by simultaneously monitoring MTs labeled with GFP-TUA6, AFs labeled
531 with Lifeact-TagRFP and stromules labeled with NRIP1(cTP)-BFP via time-lapse confocal
532 microscopy (*Figure 8B*). When our third revision version of the manuscript was under review,
533 another report has proposed a model in which both stromule extension and slow anchoring
534 occurs on MTs and rapid extension occurs on AFs (Erickson et al., 2017b). Our high-resolution
535 imaging data clearly indicate that stromules do not extend along AF. Our data shows that static
536 stromule anchoring is associated with the AF network and dynamic movement occurs along
537 MTs. We used both Lifeact and mTalin, since they may label different pools of AFs. Lifeact
538 results in even labeling of fine AF network and is accepted as one of the best markers for AF
539 (Riedl et al., 2008). However, mTalin was used previously for labeling cp–actin interacting with
540 chloroplasts and required for blue-light mediated movement (Kadota et al., 2009). We have
541 found that each marker has its own advantages and disadvantages, and no single marker is
542 perfect. The actin inhibitor CTD disrupted the actin network, briefly destabilizing stromules
543 which then dynamically re-extended along MTs. It is possible that myosin XI silencing is
544 causing a similar effect, since knockout of myosin XI in *Arabidopsis* resulted in inhibiting
545 distribution and dynamics of actin network (Cai et al., 2014; Park and Nebenfuhr, 2013).

546 Early studies examining the role of MTs during stromule formation were conducted with MT
547 inhibitors, APM or Oryzalin, leading to the conclusion that MTs have a limited role, because
548 disruption resulted in either a 25% reduction in stromule length in hypocotyls treated with 5 μM
549 of APM (Kwok and Hanson, 2003) or no alteration of stromules in *Nicotiana* leaves treated with
550 36 μM of oryzalin (Natesan et al., 2009). A recent study also shows that stromules remained

551 extended after 100 μM Oryzalin treatment (Erickson et al., 2017b). We show that both 20 μM
552 APM and 300 μM Oryzalin can disrupt stromules in *Nicotiana* leaves; and propose that the
553 difference between these studies may be caused by differences in either cell type or inhibitor
554 concentration. The plastids in epidermal pavement cells in *Nicotiana* are chloroplasts (Barton et
555 al., 2017), compared to dark grown hypocotyls that lack chlorophyll-containing plastids (Kwok
556 and Hanson, 2003). In general, the formation of stromules may vary based on differences in cell,
557 plastid, or stimulus type. We found that 20 μM of APM or 300 μM of oryzalin MT inhibitor was
558 required to observe a more complete disruption of MTs. By monitoring MTs and stromules with
559 fluorescently-tagged markers, we were able to directly observe the effect of inhibitors on MT
560 formation and found that stromules maintained interactions with small fragments of MTs, but
561 retracted after complete disruption of MTs. The study using 100 μM Oryzalin also observed that
562 stromules would remain associated to small fragments of MT (Erickson et al., 2017b). Although
563 they did not quantify changes in stromule frequency or dynamics like we describe here, they
564 qualitatively observed more fast moving, short-lived stromules. This is consistent with the
565 overall increased stromule extension velocity that we measured after 1 μM Oryzalin treatment.
566 The role of MTs during stromule extension is also supported by time-lapse confocal microscopy
567 that shows stromule tips interacted and dynamically extended along MTs. This is consistent with
568 the recent study also showing stromule extension along MTs using mOrange2-MAP4 (Erickson
569 et al., 2017b). The involvement of MTs was unexpected because of the previously implicated
570 role of AFs; therefore, we repeated these experiments with three independent MT markers, GFP-
571 TUA6, EB1-Citrine, and TagRFP-MAP-CKL6.

572 To rule out potentially indirect effects of MT drugs, we further examined the mechanistic
573 function of MTs during stromule formation by stabilizing MTs either chemically or genetically.

574 Taxol, which stabilize MTs (Schiff and Horwitz, 1980), doubled the average number of
575 stromules per chloroplasts. Furthermore, we altered MTs genetically by silencing *NbGCP4.* The
576 γ-tubulin forms a complex with γ-tubulin complex protein (GCP) such as GCP2-GCP4 to form γ-
577 tubulin ring complex (γ-TuRC) that plays an important role in MT nucleation and organization
578 (Moritz and Agard, 2001). GCP4-GCP6 subunits are not essential for γ-tubulin complex (Vinh et
579 al., 2002), but these subunits are important for stabilizing the ring complex (Guillet et al., 2011).
580 Knockdown of GCP4 in *Arabidopsis* leaf pavement cells resulted in hyper-parallel bundles of
581 MT (Kong et al., 2010). Our results showed that *NbGCP4* silencing in *N. benthamiana* leaves
582 exhibited similar changes in MT organization via SOAX analysis. The change in MT structure
583 induced by *NbGCP4* silencing was sufficient to induce stromules constitutively. Increased
584 stromule length in *NbGCP4*-silenced plants could be due to less dynamic stromules, since
585 extension and retraction velocities decreased. It is possible that the decrease in stromule
586 dynamicity is caused by a disrupted balance between MT branching and MT bundling in
587 *NbGCP4* silenced plants. These findings support that MT dynamics are a key regulator of
588 stromule formation and dynamics.

589 It has been proposed that stromules may extend via an internal force, and not along MTs or
590 AFs. Early studies have found filament-like structures in plastids and stromules, which
591 potentially could provide an outward force (Bourett et al., 1999; Lawrence and Possingham,
592 1984). Recently, stromules were shown to form *in vitro* from isolated chloroplasts (Brunkard et
593 al., 2015); but, clean chloroplast preparations resulted in only 1.1% of chloroplasts having short,
594 spontaneous stromules and a 40-fold increase in stromules after the addition of cell extracts (Ho
595 and Theg, 2016). We also have observed rapidly moving beak-like or small protrusions (Video 2,
596 red dots) that do not interact with MTs. They also resemble “chloroplast protrusions” observed in

alpine plants that form independently of MTs (Buchner et al., 2007; Holzinger et al., 2007a; Moser et al., 2015). It was recently proposed that the small, fast moving stromules moved along actin because their rate of extension was similar to myosin motors (Erickson et al., 2017b). However, when AFs were marked with Lifeact-TagRFP, we did not observe a correlation of these stromules extending along AFs (N = 73). These studies combined suggest that there may be an alternative mechanism for stromule initiation that may depend an internal force. Another alternative to cytoskeleton driven stromule formation is force derived from membrane contact sites (MCS) with the endoplasmic reticulum (Schattat et al., 2011). Stromule and ER dynamics are correlated and it is possible that MCS stabilize stromules similar to actin anchors. They propose a model in which ER MCSs or the underlying cytoskeleton dictate stromule dynamics (Schattat et al., 2011). Our findings strongly supports a role for the cytoskeleton in which stromules require a combination of MT and AF interactions. Nonetheless, the function of the MCS between stromules and ER is intriguing and may assist in transfer of proteins, lipids or small molecules.

Blue light induced-chloroplast movement in plants is driven by chloroplast actin filaments (cp-actin) (Kadota et al., 2009). The chloroplast unusual positioning 1 (CHUP1) protein recruits actin to the leading edge of chloroplasts and is required for movement. Interestingly, the N-terminal coiled-coiled domain of CHUP1 is also required to anchor chloroplasts to the plasma membrane, revealing a complex, dual role of actin during chloroplast movement and anchoring (Oikawa et al., 2008). Chloroplasts are held by a cage of AFs (Kandasamy and Meagher, 1999) and additional recruitment of cp-actin via CHUP1 potentially may inhibit stromules by forming a physical constraint. Consistent with this hypothesis, CTD treatment disrupts actin around chloroplasts causing them to lose their ellipsoid shape to become round (*Figure 8-figure*

620 *supplement 2*). Once released, chloroplasts moved in the direction of stromules extending along
621 MTs. However, complete disruption of actin using longer treatments of CTD resulted in a
622 complete disruption of all chloroplast movement, including stromule-directed movement.
623 Stromule-guided movement was also seen without CTD treatment (*Figure 8*) and appears to be a
624 novel type of organellar movement along MTs. Over 50% of all the chloroplast movement in
625 steady-state epidermal pavement cells was stromule-directed, suggesting that this type of
626 movement may significantly contribute to chloroplast movement and positioning. Interestingly,
627 stromules in the green algae, *Acetabularia*, also have been implicated in chloroplast movement
628 (Menzel, 1994), suggesting that both cp-actin and stromule-directed chloroplast movement are
629 conserved between land plants and green algae (Suetsugu and Wada, 2016).

630 We have recently shown that stromules play an important role during innate immunity and
631 programmed cell death (Caplan et al., 2015). During an immune response, chloroplasts move
632 towards the nucleus and different types of chloroplast stromule-to-nuclear connections are
633 established (Caplan et al., 2015). However, the mechanism behind perinuclear chloroplast
634 clustering and chloroplast stromule-to-nuclear interactions is unknown. Our results described
635 here using TMV-p50-induced, effector-triggered immunity indicate a role for AFs and MTs
636 during perinuclear clustering. MTs promote stromule extensions, contributing to more stromule
637 movement, while AFs provide anchors to position chloroplasts towards the nucleus. These
638 results reinforce the role for AFs as anchor points for stromules that were also previously shown
639 to exist in *Arabidopsis* hypocotyls (Kwok and Hanson, 2004b), and a recent study showing that
640 stromules are involved in maintaining contact with nuclei (Erickson et al., 2017a). Overall, our
641 results invoke a model in which, during effector-triggered immunity, MTs facilitate stromule
642 extensions and stromules bind tightly to AFs around nuclei. The role of MTs during the

643 formation of stromule-to-nuclei connections requires further studies. However, our data suggests
644 that once those connections are formed, stromules may guide or pull chloroplasts towards the
645 nucleus, which then results in perinuclear clustering of chloroplasts.

646 Results described here show that MT-mediated stromule extension and AF-mediated
647 stromule anchoring are two complementary activities during stromule formation and movement.
648 We provide mechanistic insights into how interactions with the cytoskeleton form and stabilize
649 stromules. Furthermore, we describe a new type of organellar movement along MTs that is
650 stromule-directed and reveal a mechanism for perinuclear clustering during innate immunity. In
651 the future, it will be interesting to investigate the molecular components required for stromule
652 dynamics and stromule-directed movement and importance of perinuclear chloroplast clustering
653 during innate immunity.

654

655 **Materials and Methods**

656 **Key Resources Table**

Designation	Source or reference	Identifiers	Additional information
NRIP1	PMID: 18267075; 26120031		
GCP4	This paper		
p50	PMID: 18267075; 26120031		
GV2260	PMID: 4022773		
GV3101	https://doi.org/10.1007/BF00331014		
NRIP1-Cerulean transgenic plant	PMID: 18267075; 26120031		
GFP-TUA6 transgenic plant	PMID:12084822		
FABD2-GFP transgenic plant	PMID:12084822		
NRIP-Cerulean; *N* double transgenic plant	PMID: 18267075; 26120031		
TRV1	PMID: 14501071		
TRV2-EV	PMID: 14501071		
Nicotiana benthamiana		Taxonomy ID: 4100	
mTalin-Citrine	This paper		ask construct named "SPKD2681"

Lifeact-TagRFP	This paper		ask construct named "SPKD2209"
TagRFP-MAP-CKL6	This paper		ask construct named "SPKD2386"
NRIP1(cTP)-TagBFP	This paper		ask construct named "SPKD3168"
TRV-*NbGCP4*	This paper		ask construct named "SPKD3111"
Citrine-p50-U1	This paper		ask construct named "SPKD1939"
Citrine	This paper		ask construct named "SPKD914"
p50-2xHA	PMID: 18267075; 26120031		
NLS-mCherry	PMID: 28619883		
Cytochalasin D	Sigma	C8273	
Aminoprophos-methyl (APM)	Sigma	03992	
Oryzalin	Sigma	36182	
Paclitaxel-BODIPY	Thermofisher Scientific	P7501	
DMSO	Sigma	D8418	
PRISM7	GraphPad		
Stromule detection and tracking algorithm	http://sigport.org/1807		

Plasmids

Plasmids used in this study includes mTalin-Citrine (SPDK2681), Lifeact-TagRFP (SPDK2209), TagRFP-MAP-CKL6 (SPDK2386), NRIP1(cTP)-TagBFP (SPDK3168), TRV-*NbGCP4* (SPDK3111), Citrine-p50-U1 (SPDK 1939), Citrine (SPDK914), and p50-2xHA (TBS44), NLS-mCherry. These were constructed by PCR and standard cloning methods. Details of constructions are available upon request.

Transgenic marker lines and transient expression by Agroinfiltration

Transgenic *N. benthamiana* plant expressing the NRIP1-fused to Cerulean is described in (Caplan et al., 2015; Caplan et al., 2008). Transgenic *N. benthamiana* plants expressing GFP-TUA6 and FABD2-GFP were gifts from Drs. Manfred Heinlein and Karl Oparka and described in (Gillespie et al., 2002). The plants were grown under continuous light at 20ºC on growth carts

for 4 – 5 weeks as described in (Caplan et al., 2015; Caplan et al., 2008). Cultures of GV2260 *Agrobacterium* containing the recombinant plasmids were grown on plates containing Streptomycin (50 mg/L), rifampicin (25 mg/L), and carbenicillin (50mg/L) and spectinomycin (100 mg/L) antibiotics. Agrobacterium was resuspended in infiltration media containing 10 mM $MgCl_2$, 10 mM 2-Morpholinoethanesulfonic acid (MES) and 200 μM acetosyringone and induced for at least 3 hours. Fully expanded leaves of 3 – 4 week old *N. benthamiana* were used for agroinfiltration as described in (Caplan et al., 2015; Caplan et al., 2008).

Inhibitor treatment

Actin inhibitor Cytochalasin D (200μM), microtubule inhibitors APM (20 μM) and Oryzalin (300 μM) and the microtubule stabilizing agent, Paclitaxel-BODIPY (0.8 nM) were prepared as 1M stocks in dimethyl sulfoxide (DMSO) and suspended at appropriate working concentrations in the infiltration medium prior to pressure infiltration for imaging. Working concentrations were determined after testing a range of concentrations of the respective inhibitors and agents. The concentrations that resulted in the microtubule depolymerization/stabilization without any lethal effect on the cells at the microscopic level were used further for experiments. Inhibitor treatments were performed by pressure infiltration. A small hole was made on the underside of the leaves with a razor blade. A 1 mL syringe was used to pressure infiltrate inhibitor solutions or a mock containing DMSO (≤0.2%) in infiltration media Leaf excisions approximately 4 mm^2 were taken away from the infiltration point and mounted in a Nunc coverglass bottom chamber (Thermo Fisher Scientific). The center of the sample was imaged to minimize effects caused by excision-induced wounding. All time points started immediately following the pressure infiltration of the treatment. The 0-5 min time point after the respective treatments accounts for

693 the time taken for sample preparation and mounting the samples after infiltration with the
694 inhibitors and stabilization agents.

695 For 1 hour treatment, Cytochalasin D (10 μM) and Oryzalin (1 μM) as well as DMSO (0.1%)
696 as a control were infiltrate in an area of about 3 cm diameter on the same leaf by needleless
697 syringe infiltration. After one hour, around 4 mm^2 leaf disc away from the infiltrated point were
698 excised and mounted in a Nunc coverglass bottom chamber.

699

700 **VIGS assay**

701 NRIP1-Cerulean or GFP-TUA6 *N. benthamiana* transgenic plants were used for VIGS
702 experiments as described in (Dinesh-Kumar et al., 2003). *Agrobacterium* culture containing
703 pTRV1 was mixed with culture containing TRV2-EV, or TRV2-*NbGCP4* in 1:1 ratio to adjust
704 an OD_{600} to 0.5. Plants of 6 leaf stage were infiltrated and observed their stromules were
705 observed in leaf epidermis 4 days after infiltration of VIGS vectors. In immune response
706 experiments, *Agrobacterium* culture containing TMV-p50 effector was infiltrated on the third
707 day after VIGS construct infiltration. A total of 48 images were taken from 12 plants by three
708 independent experiments for each condition. Real-time RT-PCR was performed to determine the
709 silencing efficiency. After imaging, RNA was extracted from leaves by plant RNeasy kit
710 (Qiagen) and cDNA was generated by reverse transcription using Superscript III Reverse
711 Transcriptase (Thermo-Fisher Scientific). Real time PCR was performed on a Bio-Rad CFX96
712 touch™ real-time PCR detection system (Bio-Rad) using iTaq™ Universal SYBR® Green
713 Supermix (Bio-Rad). GCP4-F-realtime 5'-GGATGGTTCATCTCATCAGC-3' and GCP4-R-
714 realtime 5'- AACAACAAGCTGCCACAGAT-3' were used for *NbGCP4* gene expression while

715 EF1α-F-Realtime 5'-CTGGTGTCCTCAAGCCTGGTATGG-3' and EF1α-R-Realtime 5'-
716 TGGCTGGGTCATCCTTGGAGTTTG-3' were used as for control PCR.
717
718 **Perinuclear clustering of chloroplasts**
719 To count chloroplast clustering under immune response, two leaves of N and NRIP1-
720 cerulean transgenic *N. benthamiana* were infiltrated with agrobacterium containing citrine 48
721 hours prior to imaging. On the same leaf, non-recombinant cell or cells containing p50-HA were
722 infiltrated 24, 30, or 36 hours before observation. 4 mm^2 leaf tissues away from the infiltrated
723 point were excised and imaged by a confocal microscope. To examine MT structure during
724 immune response, transgenic *N. benthamiana* plants containing *N and NRIP1-Cerulean* or
725 without *N and NRIP1-Cerulean* were infiltrated with Agrobacteria containing p50-HA and
726 TagRFP-MAP-CKL6 36 hours prior to imaging. For the cytoskeleton inhibitor treatment after
727 inducing immune response, transgenic *N. benthamiana* plants containing *N and NRIP1-Cerulean*
728 were infiltrated with a mixture of Agrobacteria containing p50-HA and NLS-mCherry were
729 infiltrated 35 hours before inhibitor treatment. Inhibitors were infiltrated one hour prior to the
730 imaging.
731
732 **Confocal Microscopy**
733 *N. benthamiana* leaf sections (4mm^2) away from the infiltrated point were excised, infiltrated
734 with water and imaged on a Zeiss LSM 780 upright confocal microscope, LSM 710 inverted
735 confocal microscope or LSM 880 inverted confocal microscope fitted with 40X C-Apochromat
736 water immersion objective (NA=1.2) (Carl Zeiss). The 405 nm, 458 nm, 488 nm, 514 nm, or 561
737 nm laser line was used for TagBFP, Cerulean, GFP, Citrine, or TagRFP respectively. TagBFP

738 and Cerulean were pseudo-colored cyan, Lifeact-TagRFP and mTalin-Citrine were pseudo-
739 colored magenta, and GFP-TUA6, EB1-Citrine, and TagRFP-MAP-CKL6 were pseudo-colored
740 yellow throughout the manuscript. In the perinuclear clustering experiment, Citrine for cytosol
741 and nucleus diffusion was pseudo-colored blue and mCherry with nuclear localization signal was
742 pseudo-colored blue for consistency of data presentation.
743
744 **Image Processing**
745 Huygens Professional (Scientific Volume Imaging) was used on the majority of images to
746 deconvolve using a Classical Maximum Likelihood Estimation (CLME) restoration method, to
747 remove drift using the object stabilizer algorithm, to correct photobleaching across time lapsed
748 images and to equalize brightness and contrast. Noise was removed from images that were not
749 suited for deconvolution using a 3 x 3 median filter. Volocity (Perkin Elmer) was used to
750 generate images, kymographs and videos.
751
752 **SOAX microtubule analysis**
753 Bio-filament analyzing program SOAX (Xu et al., 2015), which utilizes multiple
754 Stretching Open Active Contours (SOACs), was used in order to determine Curvature, Length
755 and Azimuthal Angles for MT filaments within Maximum Intensity Projections (MIP) of
756 epithelial leaf cells. High-resolution z-stacks were acquired on an LSM 880 confocal microscope
757 or an LSM 710 confocal microscope and deconvolved in Huygens Professional batch
758 conversion, with Regularization per channel decreased to a minimum of 2, and Quality Change
759 Threshold changed to 0.05. Resulting images were then converted into MIPs using Fiji (ImageJ)
760 and analyzed. Regions were selected from 5 maximum intensity projections for each treatment,

761 towards the central region of epidermal pavement cells which poses clear MT network. Regions
762 were uniform in a radius of 10 μm from the center point, and minor errors in regional snakes
763 were corrected. Following this, each region was analyzed using curvature and snake length
764 analysis. Points of high filament visibility and quality were analyzed within each cell. Curvature
765 and Snake Length were then compiled, while Azimuthal Angles were converted to Mean
766 Resultant Lengths for statistical analysis. All settings for SOAX analysis were kept at program
767 defaults excluding Ridge Threshold, increased to a maximum of 0.04 with a minimum of 0.02,
768 and Stretch Factor, increased to 1. Results were compiled and graphed with Prism 7 (GraphPad).
769 Azimuthal angle color-coding was performed on SOAX analyzed images to display the
770 orientation of MTs.
771
772 **Quantification of stromules**
773 Stromules were manually counted using ImageJ (National Institutes of Health, Bethesda,
774 Maryland, USA) from the maximum intensity projections of the confocal images. Mean stromule
775 ratios were determined by counting the total number of stromules and then dividing by the total
776 number of chloroplasts. To quantify perinuclear clustering, *Agrobacterium*-containing
777 p35S::Citrine T-DNA vector was infiltrated into *N. benthamiana* NRIP1-Cerulean transgenic
778 plant leaves as described in (Caplan et al., 2015; Caplan et al., 2008). Twenty-four hours later,
779 either *Agrobacterium*-containing TMV-p50 or empty vector control was infiltrated. Images in Z
780 series were captured by confocal microscope as described in (Caplan et al., 2015) at the indicated
781 time points. Perinuclear chloroplasts were counted manually with the cell counter plugin in
782 ImageJ. Experiments were repeated three times with similar results and graphed with Prism 7
783 (GraphPad).

Automated stromule tracking

Matlab code was written to perform Fuzzy c-means clustering (FCM), active contour framework, contour smoothing, unit normal feature analysis and branch analysis. In the FCM, we utilize both spectral energy and spatial energy functions for clustering. A 5 by 5 window around each pixel is used to compute the spatial component. In our experiments, we clustered the spectral domain into eight clusters and compute coefficients for each pixel. Pixels having 30% coefficients as background and 70% as the foreground were then used in the active snake formulation. Matlab code is also written to perform tracking stromule. Segmentation is first performed in 3-4 layers from total 8 layers of z stack. Results are then projected into one image to perform nearest neighbor based tracking.

Manual stromule tracking

Sixty frames of time-lapse z-stack images of stromule dynamics were acquired every 10 sec in NRIP1-Cerulean transgenic plants silenced for *NbGCP4* or vector control with and without the TMV-p50 effector. Maximum intensity projections of time-lapse z-stacks were generated in Zen software (Carl Zeiss) and motion types including, extension, retraction, constant smooth, sudden erratic, and side tangential were manually counted. The maximum and minimum stromule lengths were manually measured using the FIJI version of ImageJ (Schindelin et al., 2012). The extension and retraction velocities were calculated using the Cell Counter plugin in FIJI ImageJ, via frame-by-frame analysis. This allows quantification of movement of stromules between frames of a temporal stack, in 2D and 3D.

807 **Transmission Electron Microscopy**

808 Transmission electron microscopy was conducted as described previously in Caplan et. al.
809 (2015). Leaf excisions were fixed with 2% paraformaldehyde and 2% gluaraldehyde in PHEM
810 (60 mM PIPES, 25 mM HEPES, 10 mM EGTA, and 2 mM MgCl2, pH 6.9) buffer for 45 min)
811 overnight at 4°C. Samples were washed with 0.1 M sodium cacodylate buffer (pH 7.4), postfixed
812 with 1% osmium tetroxide in the same buffer for 2 hr, and then washed with buffer and water.
813 Samples were dehydrated in an acetone series (25%, 50%, 75%, 95%, and twice in anhydrous
814 100% acetone; 30 min each step) and infiltrated with Quetol 651-NSA resin. Ultrathin serial
815 sections were cut on a Reichert-Jung Ultracut E ultramicrotome and collected onto a film of
816 0.5% formvar using 2 × 1 single slot grids. Sections were post-stained with methanolic uranyl
817 acetate and Reynolds' lead citrate and examined with a Zeiss Libra 120 TEM operating at
818 120kV. Images were acquired with a Gatan Ultrascan 1000 2k × 2k CCD.

819

820 **Statistical Analysis**

821 Statistical analysis was performed using Microsoft Excel 2013 (Microsoft) and Prism 7
822 (GraphPad). Stromule counts were performed on 3-4 images obtained at the appropriate time
823 points depending on the drug treatment. Experiments were repeated at least three times. For
824 experiments involving the Paclitaxel-BODIPY treatment each image was considered a replicate
825 and the experiment was repeated three times. Student's t-test with Welch's correction was
826 performed to examine difference between treatments. For stromule frequency, the results passed
827 the D'Agostino & Pearson's normality test. Thus, t-test with Welch's correction was used to
828 evaluate the differences. For the stromule lengths, rank transformation was performed and Mann-
829 Whitney test was used for comparison. Comparisons of velocities of stromule extension and

retraction between all the conditions were done using Dunnett's multiple comparison. For the perinuclear clustering, non-parametric Mann-Whitney t-tests were performed to evaluate the differences. All graphs were formed with Prism 7 (GraphPad). Statistical analyses and graph generations were performed using Prism 7.

Acknowledgements

We thank Drs. Jung-Youn Lee and Bo Liu for providing MAP-CKL6 and EB1 plasmids respectively. We thank Drs. Manfred Heinlein and Karl Oparka for providing GFP-TUA6 *N. benthamiana* transgenic seeds. The National Institute of Health R01 grant GM097587 to S.P.D-K and J.L.C., supported this work. Microscopy access was supported by grants from the NIH (P20 GM103446, S10 OD016361 and S10 RR027273).

References

Avisar, D., A.I. Prokhnevsky, K.S. Makarova, E.V. Koonin, and V.V. Dolja. 2008. Myosin XI-K Is required for rapid trafficking of Golgi stacks, peroxisomes, and mitochondria in leaf cells of *Nicotiana benthamiana*. *Plant Physiol*. 146:1098-1108.

Barton, K.A., M.R. Wozny, N. Mathur, E.A. Jaipargas, and J. Mathur. 2017. Chloroplast behaviour and interactions with other organelles in *Arabidopsis thaliana* pavement cells. *J Cell Sci*. doi:10.1242/jcs.202275 (Epub ahead of print).

Ben-Nissan, G., W. Cui, D.J. Kim, Y. Yang, B.C. Yoo, and J.Y. Lee. 2008. *Arabidopsis* casein kinase 1-like 6 contains a microtubule-binding domain and affects the organization of cortical microtubules. *Plant Physiol*. 148:1897-1907.

Bourett, T.M., K. Czymmek, and R.J. Howard. 1999. Ultrastructure of chloroplast protuberances in rice leaves preserved by high-pressure freezing. *Planta*. 208:472-479.

Brunkard, J.O., A.M. Runkel, and P.C. Zambryski. 2015. Chloroplasts extend stromules independently and in response to internal redox signals. *Proc. Natl. Acad. Sci. USA* 112:10044-10049.

Buchner, O., A. Holzinger, and C. Lutz. 2007. Effects of temperature and light on the formation of chloroplast protrusions in leaf mesophyll cells of high alpine plants. *Plant Cell Env*. 30:1347-1356.

Cai, C., J.L. Henty-Ridilla, D.B. Szymanski, and C.J. Staiger. 2014. *Arabidopsis* myosin XI: a motor rules the tracks. *Plant Physiol*. 166:1359-1370.

Cai, G., L. Parrotta, and M. Cresti. 2015. Organelle trafficking, the cytoskeleton, and pollen tube growth. *J Integrat Plant Biol*. 57:63-78.

Caplan, J.L., A.S. Kumar, E. Park, M.S. Padmanabhan, K. Hoban, S. Modla, K. Czymmek, and S.P. Dinesh-Kumar. 2015. Chloroplast Stromules Function during Innate Immunity. *Dev Cell* 34:45-57.

Caplan, J.L., P. Mamillapalli, T.M. Burch-Smith, K. Czymmek, and S.P. Dinesh-Kumar. 2008. Chloroplastic protein NRIP1 mediates innate immune receptor recognition of a viral effector. *Cell* 132:449-462.

Chan, J., G.M. Calder, J.H. Doonan, and C.W. Lloyd. 2003. EB1 reveals mobile microtubule nucleation sites in Arabidopsis. *Nature Cell Biol*. 5:967-971.

Dinesh-Kumar, S.P., R. Anandalakshmi, R. Marathe, M. Schiff, and Y. Liu. 2003. Virus-induced gene silencing. *Methods Mol Biol*. 236:287-294.

Era, A., M. Tominaga, K. Ebine, C. Awai, C. Saito, K. Ishizaki, K.T. Yamato, T. Kohchi, A. Nakano, and T. Ueda. 2009. Application of Lifeact reveals F-actin dynamics in Arabidopsis thaliana and the liverwort, Marchantia polymorpha. *Plant Cell Physiol*. 50:1041-1048.

Erickson, J.L., M. Kantek, and M.H. Schattat. 2017a. Plastid-Nucleus Distance Alters the Behavior of Stromules. *Front Plant Sci*. 8:1135.

Erickson, J. L., Adlung, N., Lampe, C., Bonas, U., and Schattat, M. H. 2017b. The *Xanthomonas* effector XopL uncovers the role of microtubules in stromule extension and dynamics in *Nicotiana benthamiana*. *Plant J.* doi:10.1111/tpj.13813 (2017).

Erickson, J.L., J. Ziegler, D. Guevara, S. Abel, R.B. Klosgen, J. Mathur, S.J. Rothstein, and M.H. Schattat. 2014. Agrobacterium-derived cytokinin influences plastid morphology and starch accumulation in *Nicotiana benthamiana* during transient assays. *BMC Plant Biol*. 14:127.

Fisher, N.I., and A.J. Lee. 1983. A correlation coefficient for circular data. *Biometrika* 70:327-332.

Gillespie, T., P. Boevink, S. Haupt, A.G. Roberts, R. Toth, T. Valentine, S. Chapman, and K.J. Oparka. 2002. Functional analysis of a DNA-shuffled movement protein reveals that microtubules are dispensable for the cell-to-cell movement of tobacco mosaic virus. *Plant Cell* 14:1207-1222.

Gray, J.C., M.R. Hansen, D.J. Shaw, K. Graham, R. Dale, P. Smallman, S.K. Natesan, and C.A. Newell. 2012. Plastid stromules are induced by stress treatments acting through abscisic acid. *Plant J*. 69:387-398.

Gray, J.C., J.A. Sullivan, J.M. Hibberd, and M.R. Hanson. 2001. Stromules: Mobile Protrusions and Interconnections Between Plastids. *Plant Biol.* 3:223-233.

Guillet, V., M. Knibiehler, L. Gregory-Pauron, M.H. Remy, C. Chemin, B. Raynaud-Messina, C. Bon, J.M. Kollman, D.A. Agard, A. Merdes, and L. Mourey. 2011. Crystal structure of gamma-tubulin complex protein GCP4 provides insight into microtubule nucleation. *Nature Struct Mol Biol*. 18:915-919.

Gunning, B.E. 2005. Plastid stromules: video microscopy of their outgrowth, retraction, tensioning, anchoring, branching, bridging, and tip-shedding. *Protoplasma* 225:33-42.

Hanson, M.R., and A. Sattarzadeh. 2008. Dynamic morphology of plastids and stromules in angiosperm plants. *Plant Cell Environ*. 31:646-657.

Higa, T., N. Suetsugu, and M. Wada. 2014. Plant nuclear photorelocation movement. *J Exp Bot*. 65:2873-2881.

Ho, J., and S.M. Theg. 2016. The Formation of Stromules In Vitro from Chloroplasts Isolated from *Nicotiana benthamiana*. *PLoS One* 11:e0146489.

Holzinger, A., O. Buchner, C. Lutz, and M.R. Hanson. 2007a. Temperature-sensitive formation of chloroplast protrusions and stromules in mesophyll cells of *Arabidopsis thaliana*. *Protoplasma* 230:23-30.

Holzinger, A., G.O. Wasteneys, and C. Lutz. 2007b. Investigating cytoskeletal function in chloroplast protrusion formation in the arctic-alpine plant *Oxyria digyna*. *Plant Biol. (Stuttg)*. 9:400-410.

Kadota, A., N. Yamada, N. Suetsugu, M. Hirose, C. Saito, K. Shoda, S. Ichikawa, T. Kagawa, A. Nakano, and M. Wada. 2009. Short actin-based mechanism for light-directed chloroplast movement in Arabidopsis. *Proc. Natl Acad. Sci. USA* 106:13106-13111.

Kandasamy, M.K., and R.B. Meagher. 1999. Actin-organelle interaction: association with chloroplast in arabidopsis leaf mesophyll cells. *Cell Motil Cytoskeleton*. 44:110-118.

Kohler, R.H., and M.R. Hanson. 2000. Plastid tubules of higher plants are tissue-specific and developmentally regulated. *J Cell Sci*. 113 (Pt 1):81-89.

Kong, Z., T. Hotta, Y.R. Lee, T. Horio, and B. Liu. 2010. The γ-tubulin complex protein GCP4 is required for organizing functional microtubule arrays in *Arabidopsis thaliana*. *Plant Cell* 22:191-204.

Kumar, A., S.P. Dinesh-Kumar, and J. Caplan. 2014. Stromules. *Adv Plant Biol: Plastid Biol.* 5:189-207; Ed. Theg, S and Wollman, F.

Kwok, E.Y., and M.R. Hanson. 2003. Microfilaments and microtubules control the morphology and movement of non-green plastids and stromules in *Nicotiana tabacum*. *Plant J*. 35:16-26.

Kwok, E.Y., and M.R. Hanson. 2004a. In vivo analysis of interactions between GFP-labeled microfilaments and plastid stromules. *BMC Plant Biol*. 4:2.

Kwok, E.Y., and M.R. Hanson. 2004b. Plastids and stromules interact with the nucleus and cell membrane in vascular plants. *Plant Cell Reports*. 23:188-195.

Kwok, E.Y., and M.R. Hanson. 2004c. Stromules and the dynamic nature of plastid morphology. *J. Microscopy* 214:124-137.

Lawrence, M.E., and J.V. Possingham. 1984. Observations of microtubule-like structures within spinach plastids. *Biol. Cell*. 52:77-82.

Ledbetter, M.C., and K.R. Porter. 1963. A "Microtubule" in Plant Cell Fine Structure. *J. Cell Biol*. 19:239-250.

Li, S., T. Sun, and H. Ren. 2015. The functions of the cytoskeleton and associated proteins during mitosis and cytokinesis in plant cells. *Front Plant Sci*. 6:282.

Lu, G., L. Ren, J. Caplan, and C. Kambhamettu. 2017. Stromule branch tip detection based on accurate cell image segmentation. *IEEE SigPort*. Online: http://sigport.org/1807.

Menzel, D. 1994. An Interconnected Plastidom in *Acetabularia*—Implications for the Mechanism of Chloroplast Motility. *Protoplasma* 179:166-171.

Moritz, M., and D.A. Agard. 2001. Gamma-tubulin complexes and microtubule nucleation. *Curr Opin Struct Biol*. 11:174-181.

Moser, T., A. Holzinger, and O. Buchner. 2015. Chloroplast protrusions in leaves of *Ranunculus glacialis* L. respond significantly to different ambient conditions, but are not related to temperature stress. *Plant Cell Environ*. 38:1347-1356.

Natesan, S.K., J.A. Sullivan, and J.C. Gray. 2005. Stromules: a characteristic cell-specific feature of plastid morphology. *J. Exp Bot*. 56:787-797.

953 Natesan, S.K., J.A. Sullivan, and J.C. Gray. 2009. Myosin XI is required for actin-associated
954 movement of plastid stromules. *Mol. Plant* 2:1262-1272.
955 Oikawa, K., Yamasato, A., Kong, S.G., Kasahara, M., Nakai, M., Takahashi, F., Ogura, Y.,
956 Kagawa, T., Wada, M. 2008. Chloroplast outer envelope protein CHUP1 is essential for
957 chloroplast anchorage to the plasma membrane and chloroplast movement. *Plant Physiol.*
958 148:829-842.
959 Park, E., and A. Nebenfuhr. 2013. Myosin XIK of Arabidopsis thaliana accumulates at the root
960 hair tip and is required for fast root hair growth. *PLoS One* 8:e76745.
961 Reisen, D., and M.R. Hanson. 2007. Association of six YFP-myosin XI-tail fusions with mobile
962 plant cell organelles. *BMC Plant Biol*. 7:6.
963 Riedl, J., A.H. Crevenna, K. Kessenbrock, J.H. Yu, D. Neukirchen, M. Bista, F. Bradke, D.
964 Jenne, T.A. Holak, Z. Werb, M. Sixt, and R. Wedlich-Soldner. 2008. Lifeact: a versatile
965 marker to visualize F-actin. *Nat Methods* 5:605-607.
966 Sattarzadeh, A., J. Krahmer, A.D. Germain, and M.R. Hanson. 2009. A myosin XI tail domain
967 homologous to the yeast myosin vacuole-binding domain interacts with plastids and
968 stromules in *Nicotiana benthamiana. Mol. Plant* 2:1351-1358.
969 Schattat, M., K. Barton, B. Baudisch, R.B. Klosgen, and J. Mathur. 2011. Plastid stromule
970 branching coincides with contiguous endoplasmic reticulum dynamics. *Plant Physiol*.
971 155:1667-1677.
972 Schattat, M.H., and R.B. Klosgen. 2011. Induction of stromule formation by extracellular
973 sucrose and glucose in epidermal leaf tissue of Arabidopsis thaliana. *BMC Plant Biol*.
974 11:115.
975 Schiff, P.B., and S.B. Horwitz. 1980. Taxol stabilizes microtubules in mouse fibroblast cells.
976 *Proc. Natl Acad. Sci. USA* 77:1561-1565.
977 Schindelin, J., I. Arganda-Carreras, E. Frise, V. Kaynig, M. Longair, T. Pietzsch, S. Preibisch, C.
978 Rueden, S. Saalfeld, B. Schmid, J.Y. Tinevez, D.J. White, V. Hartenstein, K. Eliceiri, P.
979 Tomancak, and A. Cardona. 2012. Fiji: an open-source platform for biological-image
980 analysis. *Nat Methods* 9:676-682.
981 Sokal, R. R. and F. J. Rohlf 1995. Biometry: The Principles and Practice of Statistics in
982 Biological Research, W. H. Freeman.
983 Suetsugu, N., and M. Wada. 2016. Evolution of the Cp-Actin-based Motility System of
984 Chloroplasts in Green Plants. *Front Plant Sci*. 7:561.
985 Takeuchi, M., A. Staehelin, and Y. Mineyuki. 2017. Actin-Microtubule Interaction in Plants.
986 *INTECH: "Cytoskeleton - Structure, Dynamics, Function and Disease", Ed by Jimenez-*
987 *Lopez, J*. http://dx.doi.org/10.5772/66930:33-54.
988 Vinh, D.B., J.W. Kern, W.O. Hancock, J. Howard, and T.N. Davis. 2002. Reconstitution and
989 characterization of budding yeast gamma-tubulin complex. *Mol. Biol. Cell* 13:1144-1157.
990 Waters, M.T., R.G. Fray, and K.A. Pyke. 2004. Stromule formation is dependent upon plastid
991 size, plastid differentiation status and the density of plastids within the cell. *Plant J.* 39:655-
992 667.
993 Whitham, S., S.P. Dineshkumar, D. Choi, R. Hehl, C. Corr, and B. Baker. 1994. The Product of
994 the Tobacco Mosaic-Virus Resistance Gene-N - Similarity to Toll and the Interleukin-1
995 Receptor. *Cell*. 78:1101-1115.
996 Xu, T., D. Vavylonis, F.-C. Tsai, G.H. Koenderink, W. Nie, E. Yusuf, I.-J. Lee, J.-Q. Wu, and X.
997 Huang. 2015. SOAX: a software for quantification of 3D biopolymer networks. *Sci. Rep*.
998 5:9081.

999

Figure Legends

Figure 1. Chloroplast stromules extend along microtubules.

(**A**) MTs were marked by transiently expressing TagRFP-MAP-CKL6 (yellow) in *N. benthamiana* transgenic plants expressing NRIP1-Cerulean that marks stromules (cyan). Confocal micrographs of stromule-to-MT interactions in lower epidermal pavement cells are shown. Arrows indicate stromule beaking (1), tip contact (2), extension along (3), kinking (4) and branching (5) associations with MTs. Approximately 11% of stromules were not attached to MTs (2, arrowhead). Images are maximum intensity projection of confocal z-stacks. Scale bars equal 2 μm. Total of 103 stromules were observed in 11 biological replicates to generate this data. (**B**) Stromules were marked by expressing NRIP1(cTP)-TagRFP in transgenic GFP-TUA6 *N. benthamiana* plants. Time-lapse images were acquired and kymographs over 2 min were generated. Stromules were observed extending along MTs (left) and in both directions along MTs (right). Kymographs (bottom) were generated adjacent to the red lines in top images. (**C**) MTs were marked by expressing EB1-Citrine (yellow) in *N. benthamiana* transgenic lines expressing NRIP1-Cerulean that marks stromules (cyan). Stromules were observed extending with only the tip being pulled along MTs. Kymographs (bottom) were generated adjacent to the red lines in top image and show that a stromule tip translated along a MT at a constant rate and then rapidly changed direction (arrowhead). (**D**) The average velocity of stromules along MTs was calculated from manually tracked stromule tips moving along MTs marked with EB1-Citrine or GFP-TUA6. Data represented as the mean standard error of the mean (SEM), **** $p<0.0001$ by a Student's t-test with Welch's correction. (**E**) A stromule tip was tracked using a combination of fuzzy c-means and active contour algorithm, with shape analysis to calculate the length of the stromule, the tip velocity and the association with microtubules (Lu et al., 2017). Tip

1023 associations (green dots) with MTs (gray scale) were mapped over a time series. Tips not
1024 associating with MTs are depicted as red dots. Moving stromule tips were associated with MTs
1025 except when stromules were retracting (arrowhead).

1026

1027 **Figure 2: Microtubules direct stromule movement along the ER.**

1028 (**A**) The endoplasmic reticulum (ER) were marked by transiently expressing SP-Citrine-HDEL
1029 (magenta) and MTs were marked by TagRFP-MAP-CKL6 (yellow) in *N. benthamiana*
1030 transgenic lines expressing NRIP1-Cerulean that marks stromules (cyan). Confocal microscopy
1031 time-lapse images of lower epidermis of leaves indicating changes in stromule extension along
1032 MTs and push through the ER network (bottom right, merged). Arrows indicate stromule
1033 extension within an ER channel (ER) along MT. (**B**) High resolution airyscan confocal
1034 micrograph showing the interaction of the stromule (S) with the MT within the ER channel. (**C**)
1035 High resolution time-lapse images showing the extension of stromules (cyan) along the MTs
1036 (yellow) within and away from the ER channel (magenta). Arrows indicate active stromule
1037 extension while the ER follows the course of the extending stromule (203 s) followed by the ER
1038 remodeling (219 s) independent of the stromule extension. Scale bars equal 5 μm.

1039

1040 **Figure 3. Microtubule disruption lead to stromule retraction and microtubule stabilization**
1041 **increased stromules.** (**A**) Dynamics of MT depolymerization and stromule retraction in the
1042 lower epidermis of NRIP1-Cerulean transgenic *N. benthamiana* plant leaves after infiltration of
1043 mock control (0.2% DMSO) or MT depolymerizing agents, APM (20 μM) or Oryzalin (300
1044 μM). Images are maximum intensity projections represented at time points with a 5 min interval

after infiltration. Arrows in mock (top row) indicate extended and branching stromules. MT depolymerization due to APM and Oryzalin causes simultaneous stromule retraction within 15 min (arrowhead; middle and bottom panels). A beaking was initiated but failed to progress to stromule (asterisk; middle and bottom panels). Scale bar equals 2 μm. (**B**) Stromules were increased by DMSO vehicle control treatment from 0 to 15 min compared to no significant increase from the infiltration media control. Compared to the DMSO vehicle control, stromules significantly decreased after treatment with APM (20 μM) and Oryzalin (300 μM) at 15 min and no other comparisons were significant. The experiment was repeated four times with 3-5 replicates per experiment. Error bars represent mean ± standard error of the mean (SEM) **P<0.05. (**C**) Treatment with microtubule stabilizing agent Paclitaxel (0.8 nM) produced multiple stromules from single chloroplast after 30 min (arrows, bottom left panel). The extended stromules overlapped with the MTs (arrows, merged panel). Images are maximum intensity projections. Scale bar equals 5 μm. (**D**) Paclitaxel treatment increased stromules per chloroplasts after 30 min treatment compared to mock treated leaves. The experiments were repeated four times with two replicates per experiment. Error bars indicate mean ± standard error of the mean (SEM) **P<0.05 by a Student's t-test with Welch's correction.

Figure 4. Alterations of MT is correlated with NbGCP4 silencing. (**A**) In GFP-TUA6 transgenic *N. benthamiana* leaves that mark MTs (yellow), *NbGCP4* silencing resulted in hyper-parallel and occasional bundling of MT (VIGS-*NbGCP4*, right) compared to the VIGS vector control (VIGS-EV, left). Images are maximum intensity projections of confocal z-stacks. Scale bar represents 40 μm. (**B**) qRT-PCR analysis of transcript levels of *NbGCP4* in VIGS-EV control and VIGS-*NbGCP4* plants showed a significant decrease in *NbGCP4* transcript level 4

days after silencing by VIGS-*NbGCP4* compared to the VIGS-EV control. Data represented as the mean + standard error of the mean (SEM), n=12, *** P<0.001 (Student's t-test). (**C**) Azimuthal angles were analyzed by converting angles to mean resultant length (MRL) by converting the MT angles into individual vectors, adding the vectors together, and calculating the mean. MRL values are between 0 and 1, with 0 indicating that MT angles are random and 1 indicating all MT angles are the same and completely aligned. Data represented as the mean + standard error of the mean (SEM), * p<0.01 (student's t-test). (**D**) SOAX analysis was conducted on the images in (A). MT filaments are color-coded based on the azimuthal angle so that parallel MTs are the same color. (**E**) Curvature analysis that measures the rate of change of tangent vectors shows MTs in VIGS-*NbGCP4* have less curvature. Box covers from first to third quartiles while a bar in the middle of the box indicates median. Whiskers show from minimum to maximum. ****P<0.0001 by Mann-Whitney test. (**F**) Analysis of the snake length computed by SOAX analysis showed an increase in MTs length in VIGS-*NbGCP4*. Data represented as median and 95% confidence interval. **** P<0.0001 by Mann-Whitney test.

Figure 5. Microtubule stabilization induces stromules constitutively

(A) Stromules were induced 24 hours after TMV-p50 effector infiltration as described in (Caplan et al., 2015) (bottom left) compared to a mock control (top left). Stromules were induced both in mock (top right) and p50 infiltrated (bottom right) *NbGCP4*-silenced plants indicating that *NbGCP4* silencing induces stromules constitutively. Stromules were often long and branched in mock-treated *NbGCP4*-silenced plants (top right, yellow arrowheads) compared to the VIGS-EV control (top left). Scale bar represents 40 μm. **(B)** Quantitative representation of stromules from

A. Stromules were significantly induced in mock-treated *NbGCP4*-silenced plants compared to the mock-treated VIGS-EV control (compare left green bar and magenta bar). Stromules increased significantly in VIGS-EV control plants treated with p50 effector compared to the mock (compare green bars). No significant difference in stromule number was observed in *NbGCP4*-silenced mock-treated plants compared to the p50-treated plants (compare magenta bars). Four images per leaf were generated for quantification from total of 12 leaves for each condition. Data represented as the mean + standard error of the mean (SEM), ***P <0.001 (Student's t-test with Welch's correction). **(C)** Stromule length was significantly increased in mock-treated VIGS-*NbGCP4* plants compared to the VIGS-EV control (left open bars). p50 effector induced immune response increased stromule length in VIGS vector control plants compared to the mock-treated VIGS-EV control plants (compare green open bars). No significant change was observed between p50-treated and mock-treated VIGS-*NbGCP4* plants (compare red open bars). Box and whisker plot was drawn with rank transformation. Box cover from first to third quartiles while a bar in the middle of box indicates median. Whiskers show from 5 to 95 % of ranking. ***P<0.001, ♦ comparison with VIGS-EV control, p<0.001 by Mann-Whitney test. Dots in the graph indicate outliers. **(D)** The velocity of stromule extension and retraction in VIGS-EV control and VIGS-*NbGCP4* with or without TMV-p50-induced immune response. Data represented as the mean + standard error of the mean (SEM). Symbols at the top of bars indicate significant differences according to Dunnett's multiple comparison test. Single symbol (*,♦, ■), control set for each comparison; two-symbols (**,♦♦, ■■), P<0.05 and three-symbols (***,♦♦♦, ■■■), P<0.001. Scale bars equal 40 µm. **(E)** TMV-p50 induced immune response resulted in hyper-parallel MTs (*NN*+p50, right) compared to the control (*nn*+p50, left) in transgenic *N. benthamiana* leaves that mark MTs (yellow). Images are

maximum intensity projections of confocal z-stacks. Scale bar represents 20 μm. **(F)** Azimuthal angle differences of MT filaments were measured by the length of the arc. Data represented as the mean + standard error of the mean (SEM), p=0.0713 (Student's t test with Welch's correction). **(G)** Curvature analysis that measures the rate of change of tangent vectors shows MTs in *NN*+p50 have less curvature. Box covers from first to third quartiles while a bar in the middle of box indicates median. Whiskers show from minimum to maximum. ***** P<0.00001 (Mann-Whitney test). **(H)** Analysis of the snake length computed by SOAX analysis showed an increase in MTs length in *NN*+p50. Data represented as median and 95% confidence interval. *** P<0.001 by Mann-Whitney test.

Figure 6. Stromule are anchored to the actin microfilament network. (**A**) AFs were marked by expressing Lifeact-TagRFP (magenta) in *N. benthamiana* transgenic lines expressing NRIP1-Cerulean that marks stromules (cyan). Stromules were seen interacting with AFs at kink points (arrow heads). Tips were commonly seen not associated with AFs (Arrows). Stromules were occasionally seen oriented along AFs but not overlapping with AFs (*). Scale bar equals 5 μm. (**B**) An extended stromule with a tip in close proximity to an AF, became kinked at a point overlapping with an AF near the midpoint of the stromule, and retracted back to the kink point interacting with the AF. (**C**) A kymograph was created along the stromule adjacent to the 9.7 μm green line in panel B over 8 min. The stromule tip that was in close proximity to an AF and then rapidly retracts to an actin anchor. It remained attached to the actin anchor point for an additional 4 min before retraction to the body of the chloroplast. (**D**) The percent of stromules pausing at AFs during retraction events was quantified. No pausing resulted in a full retraction back to the body of the chloroplast (grey bar). Stromule retractions that did not retract completely and

paused for multiple time frames showed a correlation of the paused stromule tip with an AF (magenta bar) or no correlation with an AF (black bar). Data was collected from 22 biological replicates spanning 8 different experimental replicates. 82 retraction events were quantified from 30 different cells. Data represented as the mean + standard error of the mean (SEM), ** p <0.001, **** p<0.00001 (Student's t test with Welch's correction). (**E**) AFs were marked by expressing Citrine-mTalin (magenta) in *N. benthamiana* transgenic lines expressing NRIP1-Cerulean that marks stromules (cyan). High resolution airyscan confocal micrographs revealed thinning points of stromule or chloroplast interactions with AFs (arrowheads). Scale bar equals 2 µm.

Figure 7. Disruption of cytoskeleton change stromule dynamics. (**A**) Time lapsed images of stromules 1 hour post-treatment with 1 µM of MT inhibitor oryzalin (ORY) or with 1 µM of actin inhibitor cytochalasin D (CTD) on the leaf of the NRIP1-Cerulean transgenic *N. benthamiana.* At these concentrations, ORY disrupt MT organization slightly while no visible effect on actin cytoskeleton. On the other hand, CTD showed significant disruption of the actin filament while no significant effect on MT organization (see Figure 7-supplemental figure 1). The experiments were repeated three times with 6 replicates per treatment. Scale bar equals 20 µm. (B)-(D) Quantification of stromule dynamics in A. (B) Stromules length did not change significantly upon inhibitor treatments. (C) ORY treatment increased stromule extension velocity (magenta bars compared to green bars), while CTD treatment reduced the velocity of both stromule extension and retraction (blue bars compare to green bars). Data represented as the mean + standard error of the mean (SEM), **** p<0.0001 (Dunn's multiple comparison test). (D) The frequency of constant, smoothly extending stromules was increased (left panel) and the

frequency of sudden extending stromules decreased (right panel) with CTD treatment. ORY treatment showed no significant difference. Data represented as the mean + standard error of the mean (SEM), * $p<0.05$, (Mann-Whitney test).

Figure 8. Stromule directed chloroplast movement. (**A**) Stromules and chloroplast movement events were imaged in NRIP1-Cerulean *N. benthamiana* transgenic plants. A chloroplast was tracked (red line) in time lapsed images. The direction of movement was correlated with the direction of the stromule. A connected chloroplast (asterisk) moved with the stromule directed chloroplast. Time is measured in seconds and scale bars equal 2 μm. (**B**) AFs and stromules were marked by transiently expressing Lifeact-TagRFP (magenta) and NRIP1(cTP)-TagBFP (cyan) in *N. benthamiana* transgenic plants expressing GFP-TUA6 that marks MTs (yellow). The top row shows the merged images and the bottom row is an illustration highlighting the MT and actin dynamic events. At 0 min, the stromule tip is bound to a MT and a branch point is bound to an AF. At 1 min, the stromule extended along the MT. At 3 min, the stromule retracted to an actin anchor point. At 8 min, the stromule re-extended along a MT. At 9 min, the stromule retracted and correlated with chloroplast movement. Scale bar equals 5 μm. (**C**) The direction of the stromule connected to the chloroplast body and the direction of chloroplast movement were measured in FIJI ImageJ. The difference in angle was calculated and plotted. Both Mock and Oryzalin (ORY), showed a high frequency of values close to 0. Randomly generated values were used as a control. (**D**) The percent of chloroplast movement that were stromule directed movements were quantified. Cytochalasin D (CTD) treatment resulted in a complete halt of movement. Oryzalin (ORY) treatment caused a decrease in stromule directed movement compared to the DMSO vehicle control. Data represented as the ± SEM, ****$P<0.0001$,

1182 **P<0.01 (one-way ANOVA). (**E**) Stromules retract more frequently (ORY; pink bar) and
1183 extend less frequently (ORY; magenta bar) with oryzalin treatment. Data represented as the
1184 mean + standard deviation (SD), ***** p<0.00001 by Mann-Whitney test.

1185

1186 **Figure 9. Chloroplasts and stromules positioning during perinuclear chloroplast clustering**
1187 **during immune response.** (**A**) TMV-p50 effector and Lifeact-TagRFP (magenta; AFs) were
1188 expressed in transgenic NRIP1-Cerulean *N. benthamiana* plants that marks stromules (cyan).
1189 Time lapse images of stromule retraction towards the nucleus (N) after chloroplast positioning
1190 around the nucleus. A stromule tip (arrow head) remained stably associated with an AF
1191 associated with a nucleus and the body of the chloroplast was anchored away from the nucleus
1192 for 18 minutes. Stromule retraction from 18 to 30 min brought the chloroplast body (arrow) in
1193 close association to the nucleus. The body of the chloroplast was tracked (red line). Arrows
1194 indicate retracting stromule. Scale bar equals 5 μm. (**B**) TMV-p50 effector and Lifeact-TagRFP
1195 (magenta; AFs) were expressed in transgenic NRIP1-Cerulean *N. benthamiana* plants and then
1196 fixed as described previously (Caplan et al., 2015). Three interaction points of stromules with
1197 actin surrounding nuclei were detected (circles). The body of a chloroplast was also associated
1198 with perinuclear AFs (arrow). Image is a deconvolved maximum intensity projection of a
1199 confocal microscopy z-stack. (**C**) Enlargements of individual xy slices of the z-stack show
1200 connections of stromule tips (left) and a stromule kink point (top right) with AFs.

1201

1202 **Figure 10. Perinuclear chloroplast clustering during immune response.** (**A**) Time course
1203 images of perinuclear chloroplasts during TMV-p50 effector induced immune responses

compared to mock control. Chloroplasts and stromules marked by NRIP1-Cerulean were pseudocolored cyan while nuclei and cytoplasm were pseudocolored red. N, nucleus. Scale bar equals 20 μm. (**B**) Quantification of perinuclear chloroplasts during TMV-p50 effector induced immune response compared to mock control shown in A. Ratio of nuclei associated with more than 4 chloroplasts in TMV-p50 infiltrated cells (magenta bars) are compared to those in control cells (green bars). More than 92 nuclei were observed for each condition from 48 images. Experiments were repeated three times with 4 plants each. Data represented as the mean + standard deviation (SD), ** $p < 0.001$, * $p < 0.01$ (Student's t test with Welch's correction). (**C**) Actin cytoskeleton disruption by treatment with cytochalasin D (CTD) lead to dissociation of chloroplasts near the nucleus while microtubule disruption by treatment with oryzalin (ORY) does not affect the chloroplast positioning. Perinuclear clustering of chloroplasts was induced by TMV-p50 effector. Images were acquired 36 hours after induction. Cytoskeleton Inhibitors were treated 35 hours after induction. Chloroplasts and stromules presented by NRIP1-Cerulean were pseudocolored cyan while nuclei were pseudocolored red. N, nucleus. Scale bar equals 20 μm. (**D**) Quantification of cells associated with more than 4 chloroplasts in C. More than 60 nuclei were observed for each condition from 12 images. Experiments were repeated three times with 2 plants each (total 6 plants). Data represented as the mean + standard deviation (SD), ** $p < 0.001$ (Student's t test with Welch's correction). D, DMSO; O, oryzalin; C, cytochalasin D.

Supplement Figure Legends

Figure 1-figure supplement 1. Transmission electron microscopy of stromule-to-microtubule interactions. (**A**) Stromules were induced by transiently expressing the p50 effector for 42h in plants containing the N immune receptor. Serial sections were obtained and an overview montage image showing the position of stromules (S) in relation to the body of the chloroplast (Ch), mitochondrion (M), and nucleus (N). Scale bar equals 2 μm. (**B**) A magnified view of blue boxed area in A showing two stromules (S1, S2). (C) A further magnified area of the cyan boxed area in B shows close proximity of microtubules (gold arrow heads) along the side of a stromule (S1) and along the tip of a stromule (S2). (D, E) Two serial sections are shown to show the continuation of the close proximity of stromules to microtubules.

Figure 4-figure supplement 1. Plant morphology at different days post-silencing of NbGCP4 in NRIP1-Cerulean expressing *N. benthamiana* plants. (**A**) Plants after 4 days of virus induced gene silencing of *NbGCP4* (VIGS-*NbGCP4*) showed no detectable growth or morphological phenotype compared to VIGS vector (VIGS-EV) control plants. (**B**) Plants after 6 days of VIGS-*NbGCP4* showed a growth defect and crinkled leaves compared to the VIGS-EV control plants. (**C**) Stromule induction and branched stromule phenotype in VIGS-*NbGCP4* cells was more pronounced after 6 days of silencing compared to VIGS-EV control. However, NRIP1-Cerulean leaked out of chloroplasts and accumulated in the cytosol (arrowhead) and nucleus (arrow). (**D**) Plants after 14 days of *NbGCP4* silencing showed growth arrest and variegated leaves. Each silencing experiment included 4 plants for VIGS-*NbGCP4* and VIGS-EV. Experiment was repeated 3 times.

Figure 5-figure supplement 1. Quantitative analysis of stromule length and movements. (**A**) Stromule length was manually measured in ImageJ. Consistent with the independent measurement presented in Fig. 5C, silencing of *NbGCP4* (VIGS-*NbGCP4*) resulted in a higher percentage of stromules that were 3 μm or longer (pink) compared to VIGS empty vector (EV) control silenced plants. Total of 302, 162, 137, and 109 stromules were measured for VIGS-EV, VIGS-*NbGCP4*, VIGS-EV with TMV-p50, and VIGS-*NbGCP4* with TMV p50, respectively. Fisher's exact test was performed for comparison. *P<0.05 and ***P<0.0001. (**B**) Three types of stromule movement were manually tracked. More stable extension of stromule tips (green dot) was observed a smooth, constant motion with a linear trajectory (green line) (top row). Rapidly extending and retracting stromule tips (yellow dot) were sudden and produced an erratic trajectory (yellow line) (middle row). Stromule tips (magenta dot) moving sideways had no extension and moved tangential (magenta line) to the body of the chloroplast (bottom row). (**C**) Stromule movement types depicted in B were counted and the frequency of constant, smoothly extending stromules (green) was higher in *NbGCP4*-silenced samples. Total of 337, 186, 134, and 127 movements of stromules were recorded for VIGS-EV, VIGS-*NbGCP4*, VIGS-EV with TMV-p50, and VIGS-*NbGCP4* with TMV p50, respectively. Chi-square test was performed to compare. *P<0.05, **P<0.001.

Figure 6-figure supplement 1. Chloroplast stromules statically interact with actin microfilaments. (**A**) AFs were marked by expressing Lifeact-TagRFP (magenta) in *N. benthamiana* transgenic lines expressing NRIP1-Cerulean that marks stromules (cyan). Stromules were seen in close proximity to AFs (left). Magnified image (top right) and profile lines of fluorescence intensity (bottom right) show stromules do not overlap with AFs. Images are deconvolved confocal micrographs. Scale bars equal 2 μm. (**B**) Three additional

representative examples showing an extended stromules (top row) that partially retracted to an AF (middle row) before fully retracting (bottom row). Example 1 shows a clear kink in the stromule similar to the example in Figure 6. Examples 2 and 3 show stromules that are slightly curved that partially retract near to the location of curvature. Scale bar equals 5 μm.

Figure 6-figure supplement 2. Characterization of actin microfilaments associated with stromules and the body of chloroplasts. (**A**) Stromules were induced by transiently expressing the TMV-p50 effector for 42h in plants containing the N NLR immune receptor. A transmission electron micrograph overview montage showing the position of stromules (S) in relation to the body of the chloroplast (Ch), mitochondrion (M), and nucleus (N) can be found in Figure 1-figure supplement 1. Serial sections were acquired, and in one section a stromule with a kink (K) was seen associated with an AF bundle. (**B**) A magnified view of the boxed area (green) in A shows the close proximity of the AF bundle (arrowheads) with a stromule kink (K). Scale bar equals 2 μm. (**C**) The z-stack of confocal microscopy data represented Figure 6D was rendered in the Amira software package. The AF network was skeletonized (magenta) and thick bundles were volume rendered (orange). NRIP1-Cerulean (Cyan) in the chloroplast stroma was surface rendered. (**D**) The surface rendering of the NRIP1-Cerulean show grooves (arrows) along the body of the chloroplasts that correspond to the location of AFs. Thinning of the stromules was also evident (arrowhead).

Figure 6-figure supplement 3. Disruption of actin filaments does not affect stromule number. (**A**) AFs were marked by transiently expressing Citrine-mTalin (magenta) in *N.*

benthamiana transgenic lines expressing NRIP1-Cerulean that marks stromules (cyan). Leaves were infiltrated with either Cytochalasin D (CTD; 200 μM) or a mock control. Arrows indicate free ends of the stromules in Mock and CTD treatments. Arrowhead indicates stromule in a loop attached to the plastid body after the treatment with CTD. Images are maximum intensity projections of deconvolved confocal z-stacks. Scale bars equal 10 μm. (**B**) CTD or mock (M) solution was infiltrated in leaves and imaged immediately (0-5 min) or after 30 min of treatment. There was no significant difference in stromule numbers following CTD treatment compared to mock control. The experiments were repeated more than 3 times. A total of 176, 208, 188, and 175 stromules from 320, 344, 310, and 297 chloroplasts were recorded for mock at 0-5 min, CTD 0-5 min, mock 30 min, and CTD 30 min after treatment respectively. Data was collected from 15 maximum intensity z-stack projections from 5 biological replicates for each condition. Error bars indicate mean ± standard error of the mean (SEM). ns, not significant at P=0.7943 and P=0.9894, respectively (Student's t-test).

Figure 7-figure supplement 1. Effects of inhibitor treatments on the disruption of cytoskeleton. *N. benthamiana* GFP-TUA6 transgenic plants were used to mark microtubule (MT, yellow) and *N. benthamiana* FABD2-GFP transgenic plants were used for actin filament (AF, magenta). Treatment with 1 μM Oryzalin (ORY) for one hour generated diffusion of GFP fluorescence and short MT fragments (top middle panel) compared to 0.1% DMSO control (top left panel). At this concentration of ORY, there was no major effect on AF compared to DMSO treatment (bottom left and middle panels). Treatment with 10 μM cytochalasin D (CTD) for one hour completely abolished actin cytoskeleton (bottom right panel) compared to DMSO control

(bottom left panel). At this concentration of CTD, MT organization is relatively same as control (top right and left panels). All scale bars are 20 μm.

Figure 8-figure supplement 1. Stromule directed movement. (**A**) Stromules and chloroplast movement events were imaged in NRIP1-Cerulean *N. benthamiana* transgenic plants. (**B**) The orientation angle of the stromule connected to the chloroplast body (X-axis) and the movement of the chloroplast body (Y-axis) were plotted for the DMSO vehicle control, Oryzalin (ORY) treatment, and randomly generated control.

Figure 8- figure supplement 2. Stromule-directed chloroplast movement during partial actin disruption. (**A**) AFs and MTs were marked by transiently expressing Citrine-mTalin (magenta) and TagRFP-MAP-CKL6 (yellow) in *N. benthamiana* transgenic plants expressing NRIP1-Cerulean that marks stromules (cyan). Time-lapse images of lower epidermal pavement cells of leaves indicated changes in stromule and chloroplast movement after treatment with Cytochalasin D (200 μM). Stromules were retained early (3 min) after treatment with Cytochalasin D and then briefly disrupted (8 min) with rounding of chloroplasts. Stromules re-extended (23 min) and then initiated movement of the chloroplast body (53 min). The chloroplast body moved in the direction of stromule trajectory (58 min). Arrowheads point to the chloroplast body anchored to a fragment of actin. Arrows point to stromules. Scale bar equal 10 μm. (**B**) Stromules and chloroplasts were tracked using the algorithm described in (Lu et al., 2017). The chloroplasts on the left in panel A had two stromules (green) resulting in opposing forces and minimal movement of the chloroplast body (red). (**C**) A single stromule(green) from the

chloroplast on the right in panel A resulted in a rapid pulling of the chloroplast body (red). The image series in B and C span a 3 min interval of video 7.

Figure 9-figure supplement 1. Stromule association with perinuclear actin microfilaments. (**A**) TMV-p50 effector and Citrine-mTalin (magenta; AFs) were expressed in transgenic NRIP1-Cerulean *N. benthamiana* plants that marks stromules (Cyan). Stromules interacted with AFs associated with nuclei. Scale bar equals 5 μm. (**B**) Enlargements boxed in A showing stromule tips associated with perinuclear AF. The stromule channel (Cerulean, top row) and actin channel (magenta, middle row) are shown separately and merged (bottom row). Scale bar equals 2 μm.

Figure 10-figure supplement 1. Perinuclear clustering of chloroplasts in TMV-p50 effector induced immune response. (**A**) Frequency map of nuclei associated with different number of chloroplasts in three time points after induction of immunity by TMV-p50 effector. Nucleus number with more than 4 chloroplasts were increased from 24 hours to 36 hours after induction (red, orange, and yellow in bars). (**B**) Frequency of nucleus clustered with more than 4 chloroplasts were decreased upon actin filament inhibitor, cytochalasin D (C), while microtubule inhibitor, Oryzalin (O) showed no difference from control (0.1% DMSO; D).

Video Legends

Video 1. Stromules extend along microtubules. Stromules were marked by expressing NRIP1(cTP)-TagRFP (Cyan) in GFP-TUA6 (yellow) transgenic *N. benthamiana* plants. Time-

lapse confocal microscopy was used to acquire images every 0.92 seconds that are displayed at 30 frames/second. The first half of the video (148 frames) shows a single stromule extending along microtubules and the second half (164 frames) of a stromule moving bidirectionally along microtubules. This video was used to generate the kymographs in Figure 1B.

Video 2. Tracking of stromule tip interactions along MTs. The first half of the video shows maximum intensity projections of time-lapse confocal microscopy of 120 images taken every 8.1 seconds and displayed at 8 frames/second. MTs were marked by expressing EB1-Citrine (yellow) in transgenic *N. benthamiana* plants expressing NRIP1-Cerulean that marks stromules (cyan). Chlorophyll autofluorescence is pseudo-colored in red. Stromules were observed extending with only the tip being pulled along MTs. The second half of the video shows the tracking of stromule tips using the method described in Figure 1-figure supplement 1. The contours of stromules were defined in blue. The tip associations (green dots) with microtubules (grayscale) and non-associating tips (red dots) were mapped over a time series. The video was used to generate Figure 1C-E.

Video 3. Stromule move in channels of ER along MTs. Video show stromules (cyan) first moving along MTs (yellow) to show dynamic association, then merged with the ER (magenta), and with stromules and ER only to show movement through ER channels. The video was used to generate Figure 2A.

Video 4. Stromules remodeling ER. Stromules (cyan) move along MTs (yellow) remodeling the ER (magenta). Video was created from three consecutive time series and was used to generate Figure 2B-C.

Video 5. Stromule dynamics are disrupted by APM or Oryzalin MT inhibitor treatment.

Disruption of MT (yellow) by APM (20 μM) resulted in a loss of stromule extensions (middle) compared to the mock treatment control (left). Disruption of MT (yellow) by Oryzalin (300 μM) resulted in a loss of stromule extension compared to the mock treatment control (left). Maximum intensity projections of time-lapse z-stacks were taken every 40 seconds for Mock and Oryzalin and every 29 seconds for APM. Videos are 143 fames displayed at 15 frames per second. The video was used to generate Figure 3A.

Video 6. Stromules do not extend along AFs.

Stromules (cyan) interacted with AFs (magenta) at points along the stromule, but stromules did not directly extend along AFs. 60 images were captured by time-lapse confocal microscopy every 18 seconds and displayed at 8 frames per second. The video was used to generate Figure 6A.

Video 7. Stromule retraction to actin anchor points.

Two stromules (cyan) retracted to multiple actin anchor points (arrows) along AFs (magenta). 37 images were captured by time-lapse confocal microscopy every 18 seconds and displayed at 12 frames per second. The video was used to generate Figure 6B-C.

Video 8. Stromule-directed movement.

Chloroplast bodies and stromules were visualized in a NRIP1-CFP transgenic N. benthamiana plants, in combination with chlorophyll autofluorescence. Time-lapse confocal microscopy was

used to acquire images every 10 seconds for 600 seconds, displayed at 8 frames per second. In upper right corner an instance of stromule directed movement can be observed, which was used to generate Figure 8A. The chloroplast located in the bottom-center of the video, shows another instance of stromule-directed movement.

Video 9. Dynamic control of stromules by extension along MTs and anchoring to AFs.

AFs and stromules were marked by transiently expressing Lifeact-TagRFP (magenta) and NRIP1(cTP)-TagBFP (cyan) in *N. benthamiana* transgenic lines expressing GFP-TUA6 that marks MTs (yellow). 16 maximum intensity projections of time-lapse z-stacks taken were taken every 24.5 seconds and displayed at 4 frames per second. The video was used to generate Figure 8B.

Video 10. Chloroplasts and stromule dynamics following ORY and CTD treatments.

Chloroplast bodies and stromules were visualized in a NRIP1-CFP transgenic *N. benthamiana* plants, in combination with chlorophyll autofluorescence. Time-lapse confocal microscopy was used to acquire images every 10 seconds for 350 seconds, displayed at 16 frames per second. Displays chloroplast and stromule activity within plants subjected to either DMSO vehicle control (left), 1 μm of ORY (center), or 1 μm of CTD (right) drug treatments.

Video 11. Stromule directed movement in Cytochalasin D treated cell.

Stromules (cyan) from two chloroplasts are disrupted after Cytochalasin D treatment that fragmented AFs (magenta). Stromules re-extended along MTs (yellow) resulting in the

movement of chloroplasts. 105 maximum intensity projections of time-lapse z-stacks were taken every 39 seconds and displayed at 8 frames per second. The video was used to generate Figure 8-figure supplement 2.

Video 12. Stromule retraction resulted in the movement of a chloroplast to a nucleus. A stromule (cyan) attached to an AF (magenta) pulls the chloroplast body to the nucleus by retracting. 100 maximum intensity projections of time-lapse z-stacks were taken every 38 seconds and displayed at 8 frames per second. The video was used to generate Figure 9A.

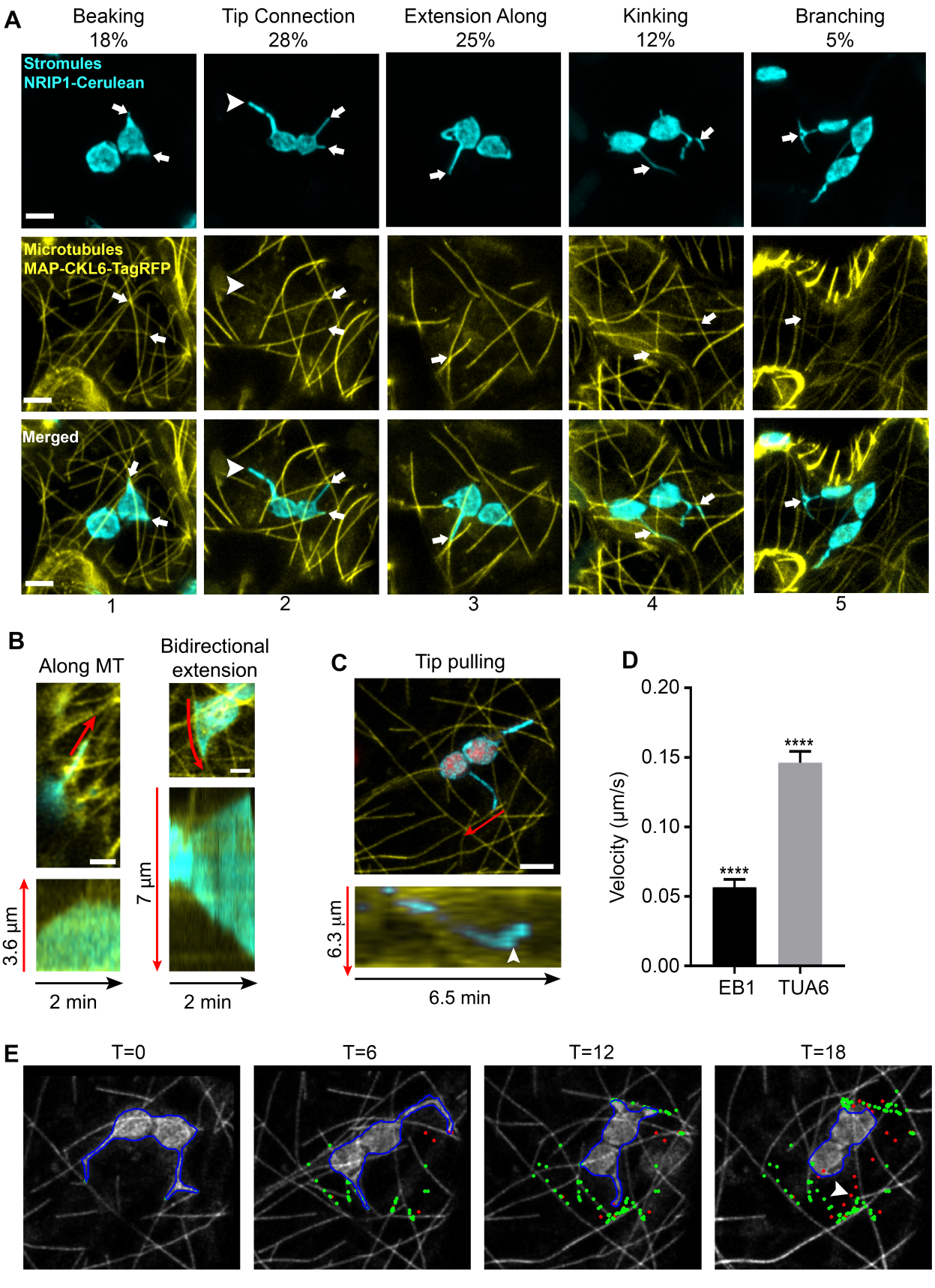
A
Beaking
18%
Tip Connection
28%
Extension Along
25%
Kinking
12%
Branching
5%
Stromules
NRIP1-Cerulean
Microtubules
MAP-CKL6-TagRFP
Merged
1
2
3
4
5
B
Along MT
Bidirectional
extension
3.6 µm
7 µm
2 min
2 min
C
Tip pulling
6.3 µm
6.5 min
D
Velocity (µm/s)
0.20
0.15
0.10
0.05
0.00
****
****
EB1
TUA6
E
T=0
T=6
T=12
T=18

Figure 1-figure supplement 1

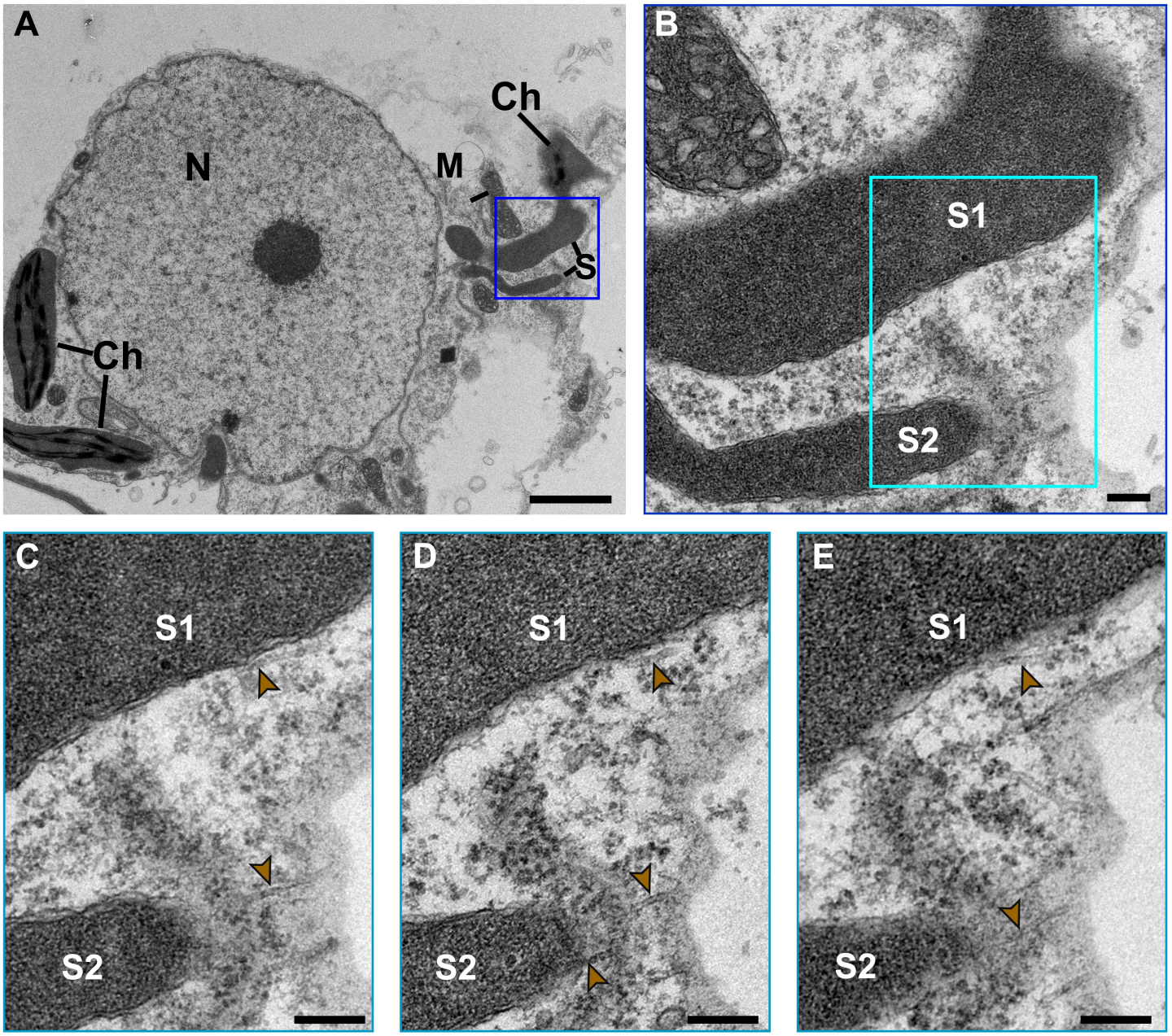

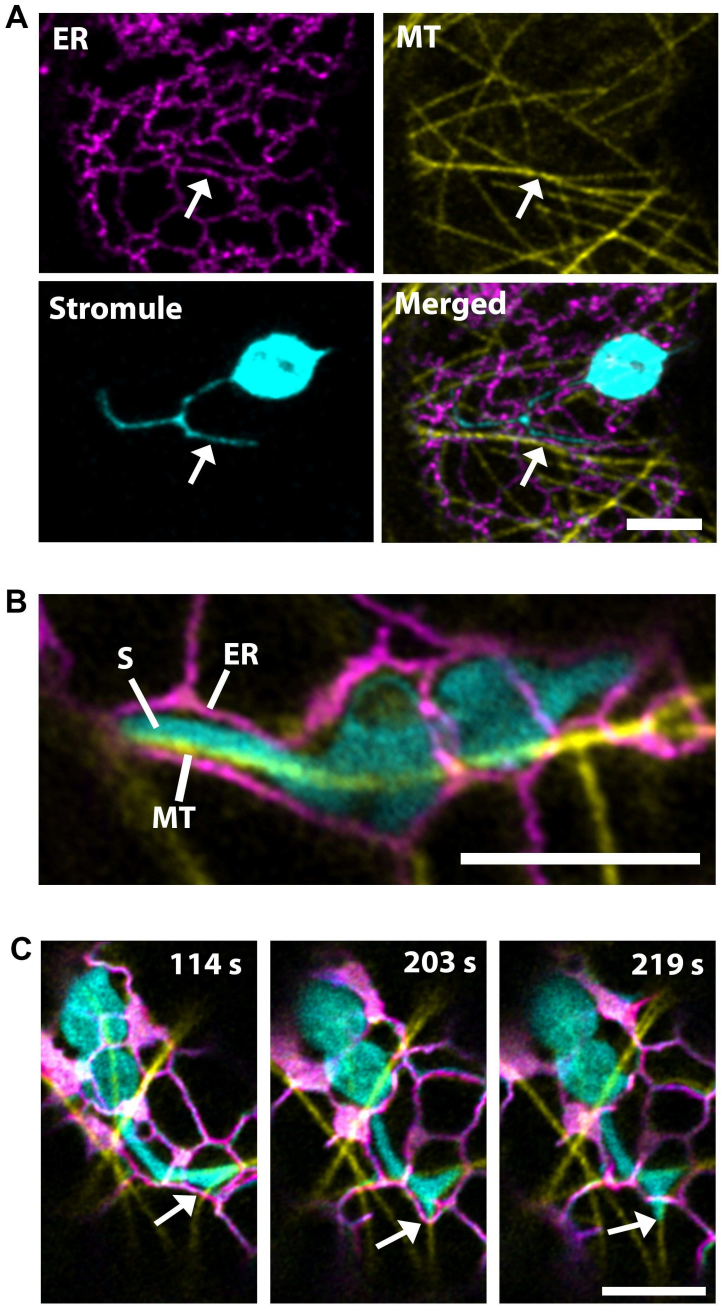
A
ER
MT
Stromule
Merged
B
S
ER
MT
C
114 s
203 s
219 s

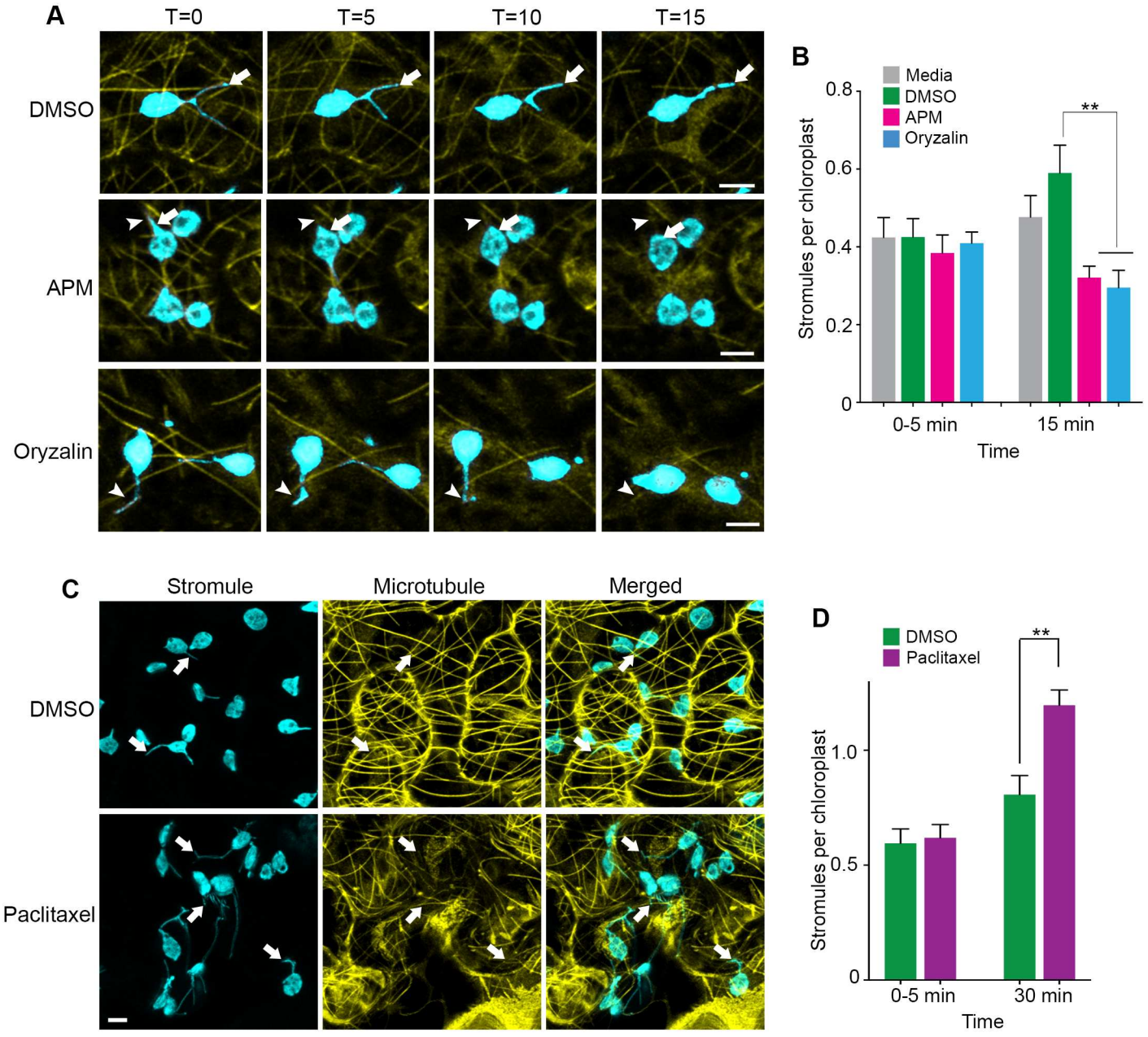
A
T=0
T=5
T=10
T=15
DMSO
APM
Oryzalin
B
Media
DMSO
APM
Oryzalin
Stromules per chloroplast
0.8
0.6
0.4
0.2
0
**
0-5 min
15 min
Time
C
Stromule
Microtubule
Merged
DMSO
Paclitaxel
D
DMSO
Paclitaxel
Stromules per chloroplast
1.0
0.5
0
**
0-5 min
30 min
Time

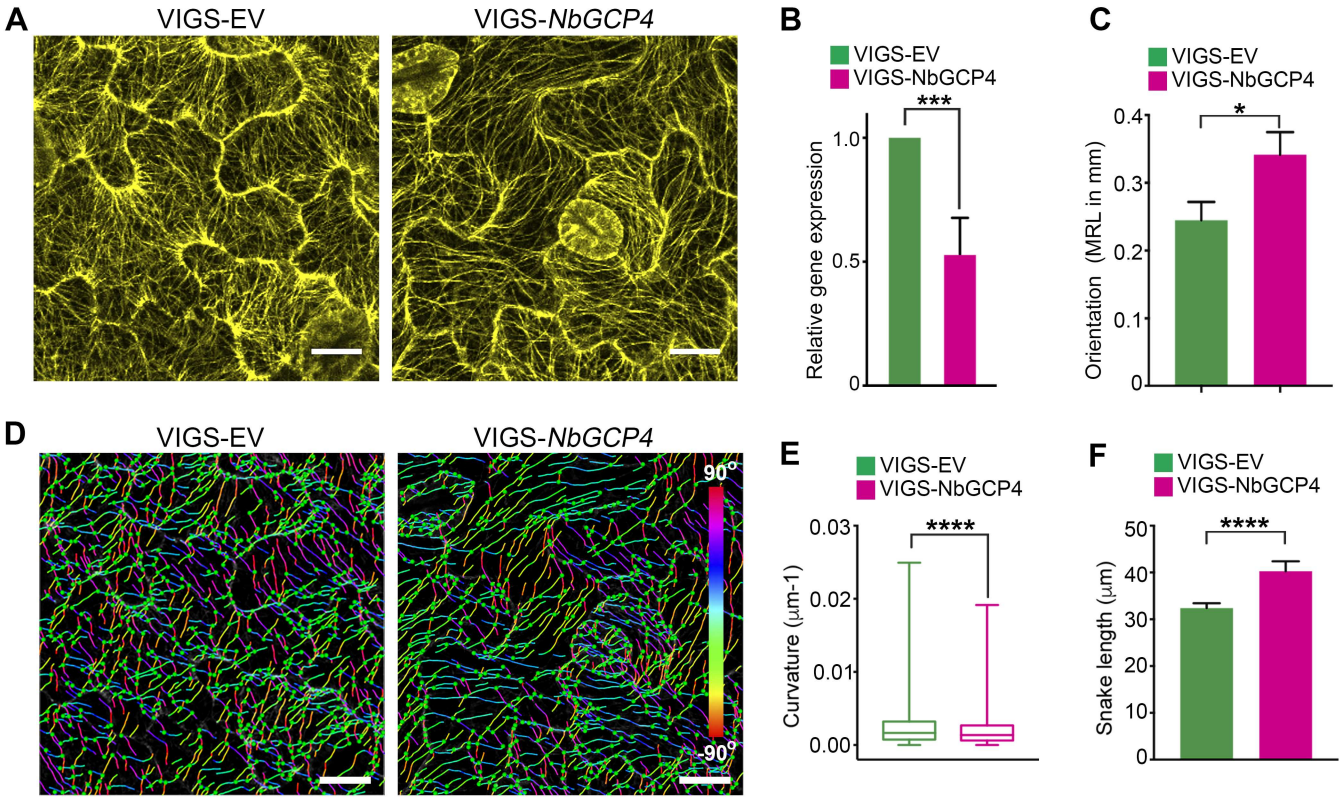
A
VIGS-EV
VIGS-NbGCP4
B
VIGS-EV
VIGS-NbGCP4
***
Relative gene expression
1.0
0.5
0
C
VIGS-EV
VIGS-NbGCP4
*
Orientation (MRL in mm)
0.4
0.3
0.2
0.1
0
D
VIGS-EV
VIGS-NbGCP4
90°
-90°
E
VIGS-EV
VIGS-NbGCP4
****
Curvature (μm-1)
0.03
0.02
0.01
0.00
F
VIGS-EV
VIGS-NbGCP4
****
Snake length (μm)
50
40
30
20
10
0

Figure 4- figure supplement 1

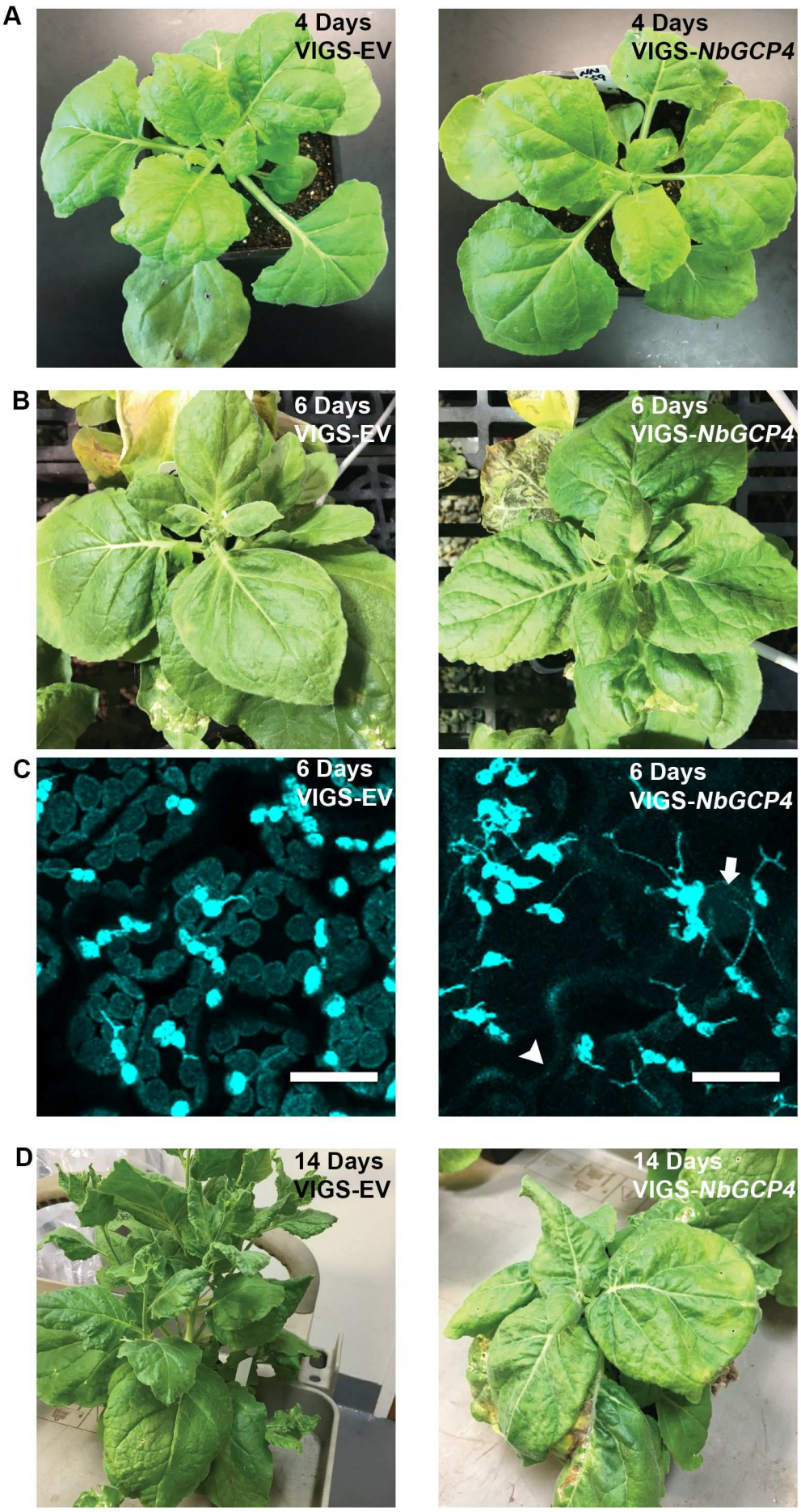

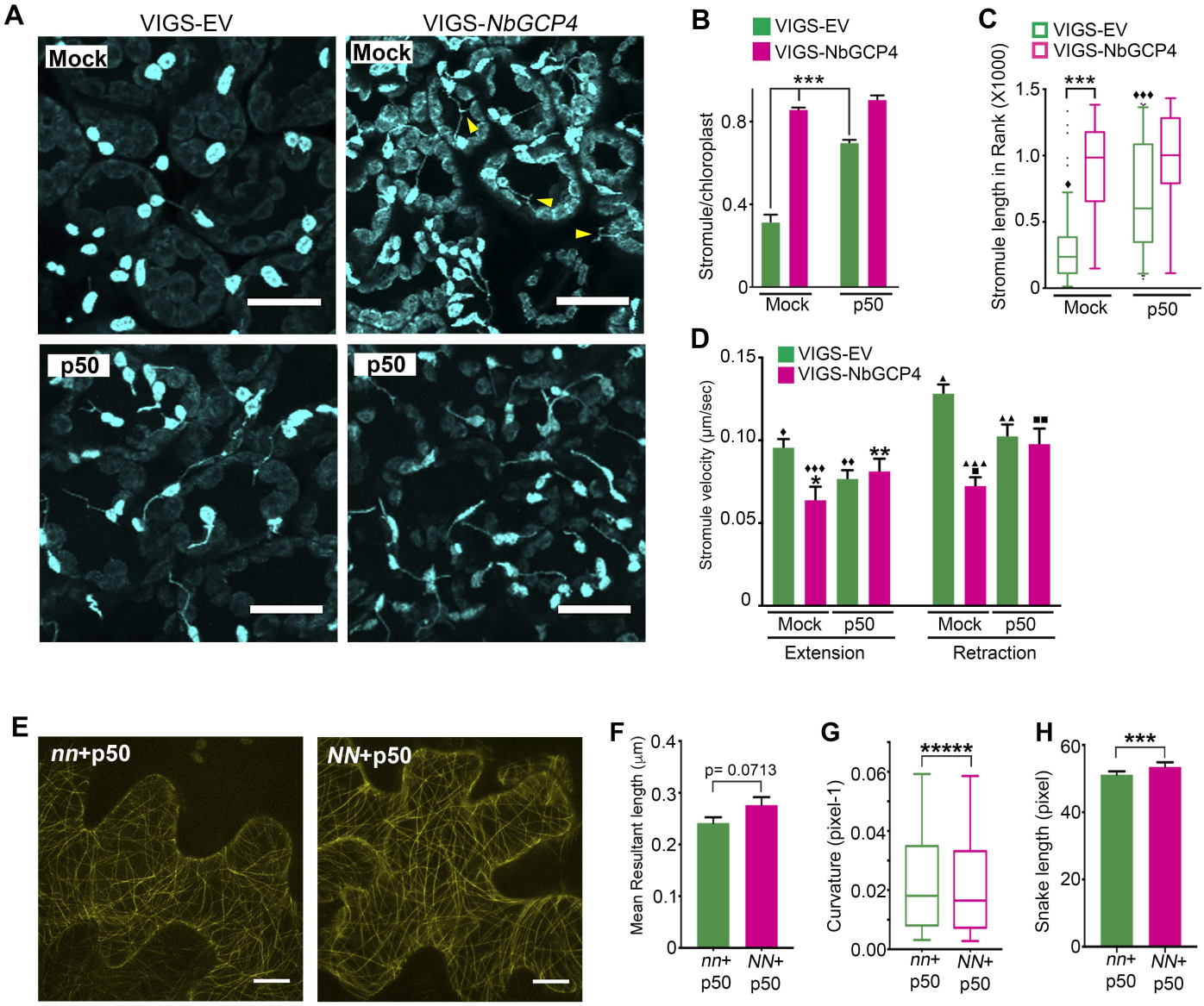
A
VIGS-EV
VIGS-NbGCP4
Mock
Mock
p50
p50
B
VIGS-EV
VIGS-NbGCP4
***
Stromule/chloroplast
0
0.4
0.8
Mock
p50
C
VIGS-EV
VIGS-NbGCP4
***
Stromule length in Rank (X1000)
0
0.5
1.0
1.5
Mock
p50
D
VIGS-EV
VIGS-NbGCP4
Stromule velocity (μm/sec)
0
0.05
0.10
0.15
Mock
p50
Mock
p50
Extension
Retraction
E
nn+p50
NN+p50
F
p= 0.0713
Mean Resultant length (μm)
0
0.1
0.2
0.3
0.4
nn+ p50
NN+ p50
G
*****
Curvature (pixel-1)
0.00
0.02
0.04
0.06
nn+ p50
NN+ p50
H
***
Snake length (pixel)
0
20
40
60
nn+ p50
NN+ p50

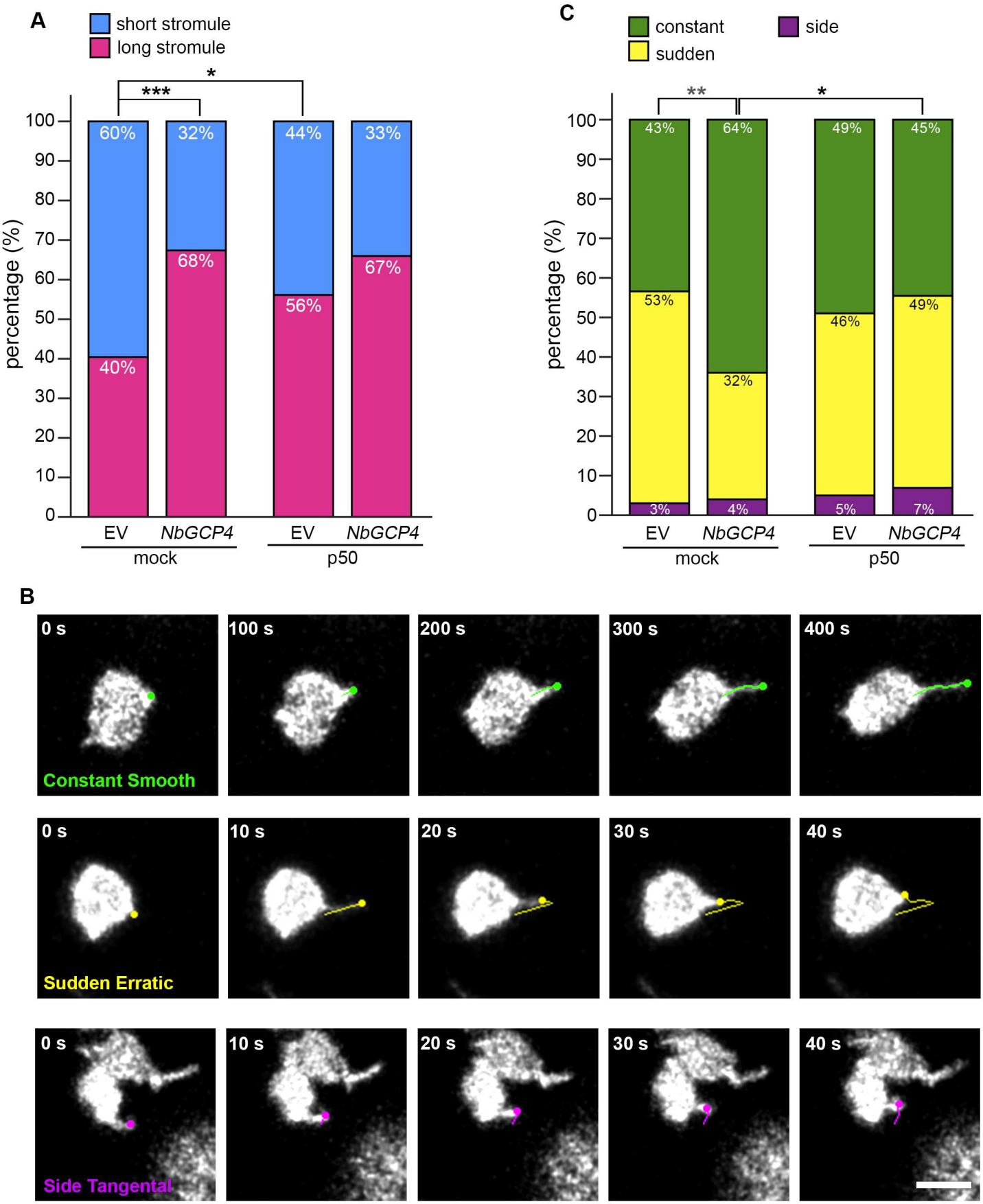
A
short stromule
long stromule
*
***
percentage (%)
100
90
80
70
60
50
40
30
20
10
0
60%
40%
32%
68%
44%
56%
33%
67%
EV
NbGCP4
EV
NbGCP4
mock
p50
C
constant
side
sudden
**
*
43%
53%
64%
32%
49%
46%
45%
49%
3%
4%
5%
7%
EV
NbGCP4
EV
NbGCP4
mock
p50
B
0 s
100 s
200 s
300 s
400 s
Constant Smooth
0 s
10 s
20 s
30 s
40 s
Sudden Erratic
0 s
10 s
20 s
30 s
40 s
Side Tangental

Figure 6

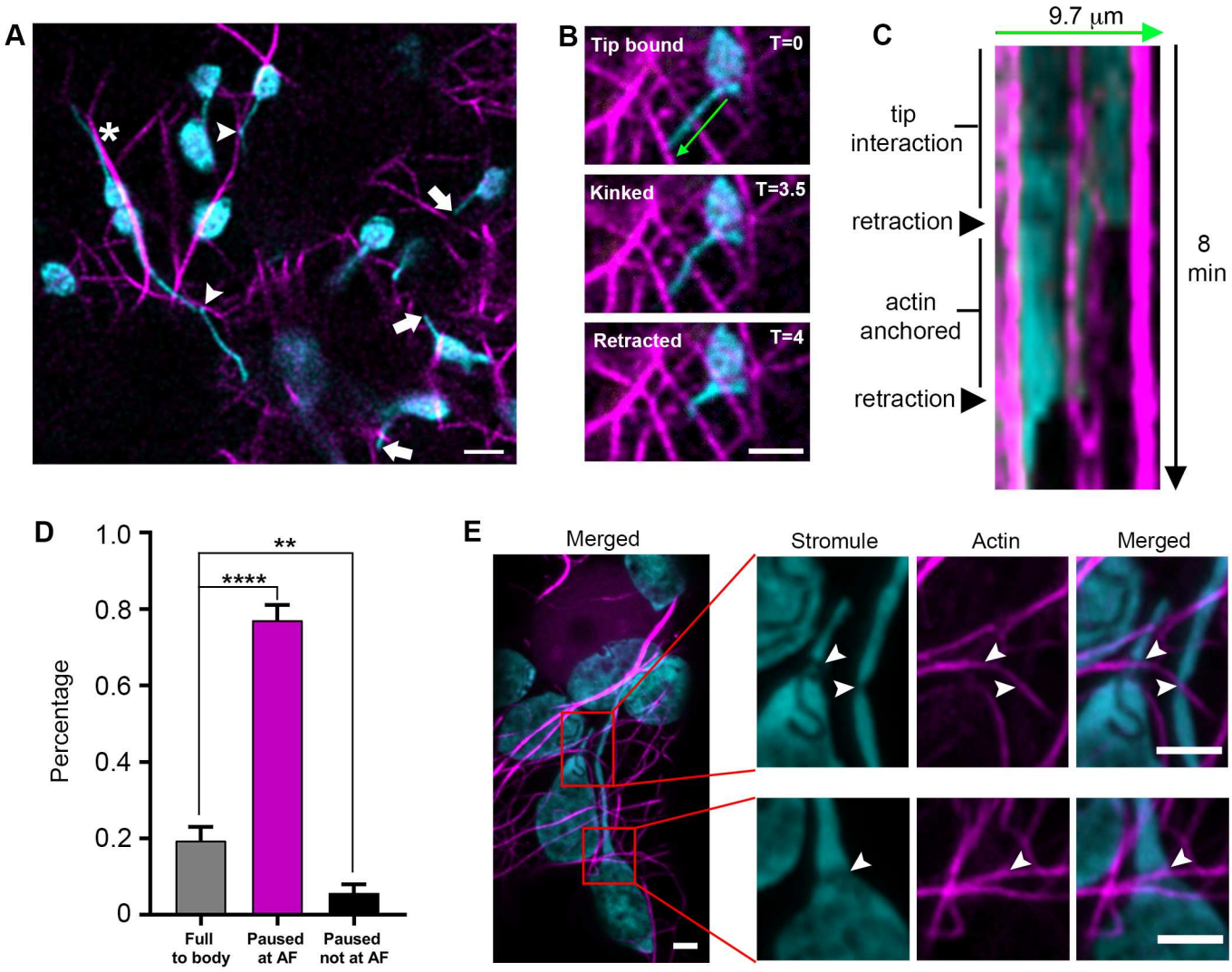
A
B
Tip bound
T=0
Kinked
T=3.5
Retracted
T=4
C
9.7 μm
tip interaction
retraction
actin anchored
retraction
8 min
D
Percentage
1.0
0.8
0.6
0.4
0.2
0
**
****
Full to body
Paused at AF
Paused not at AF
E
Merged
Stromule
Actin
Merged

Figure 6-figure supplement 1

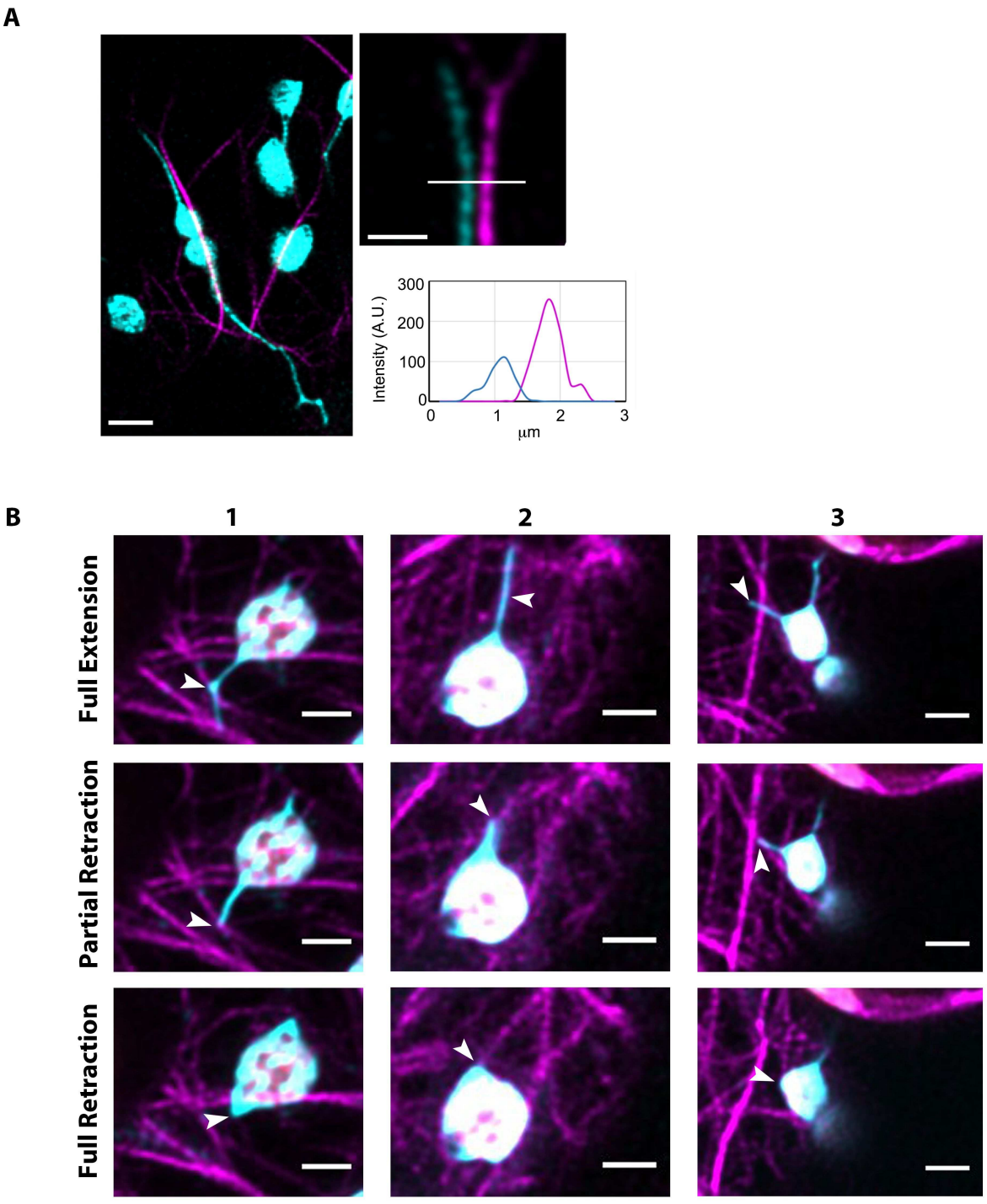

Figure 6-figure supplement 2

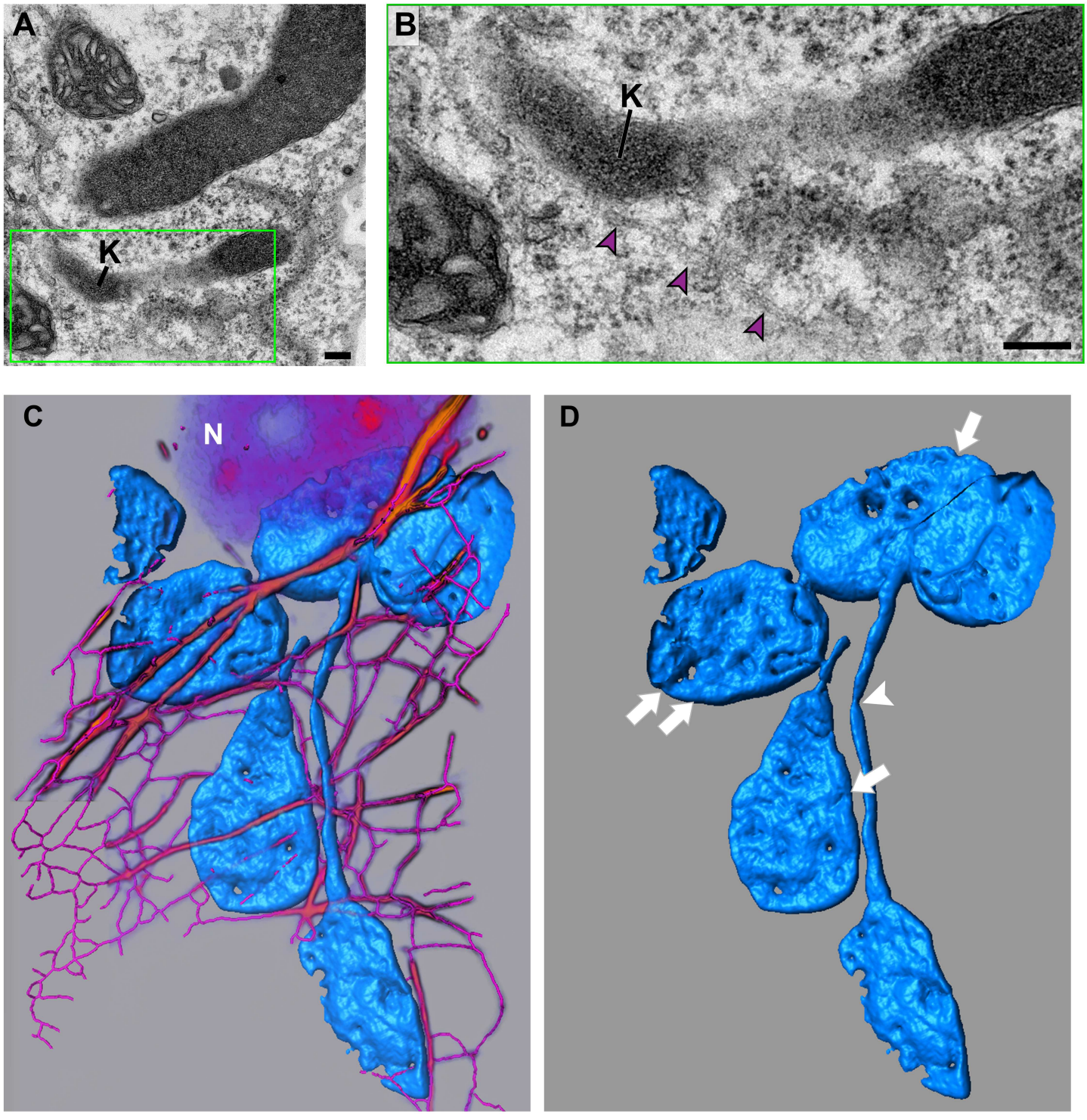

Figure 6-figure supplement 3

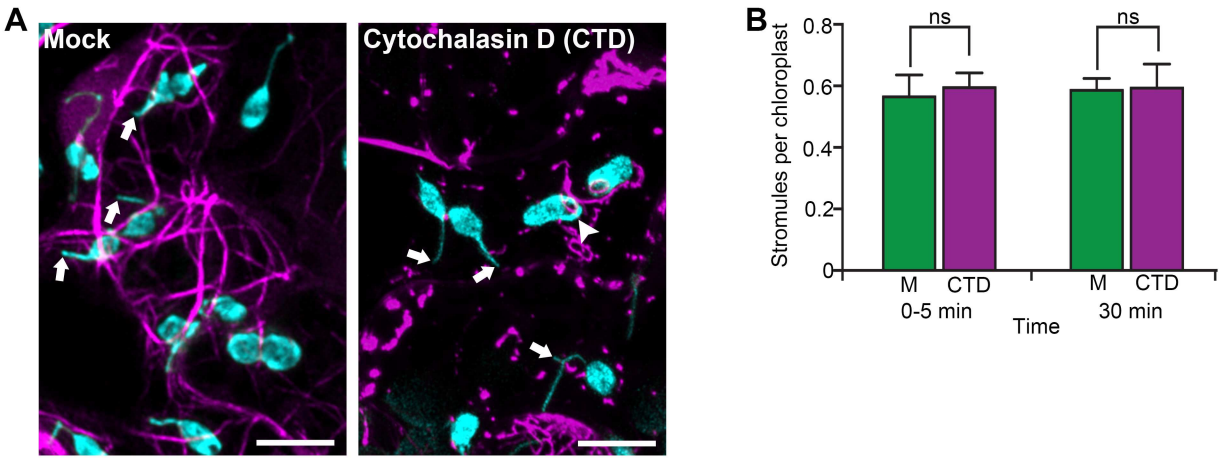

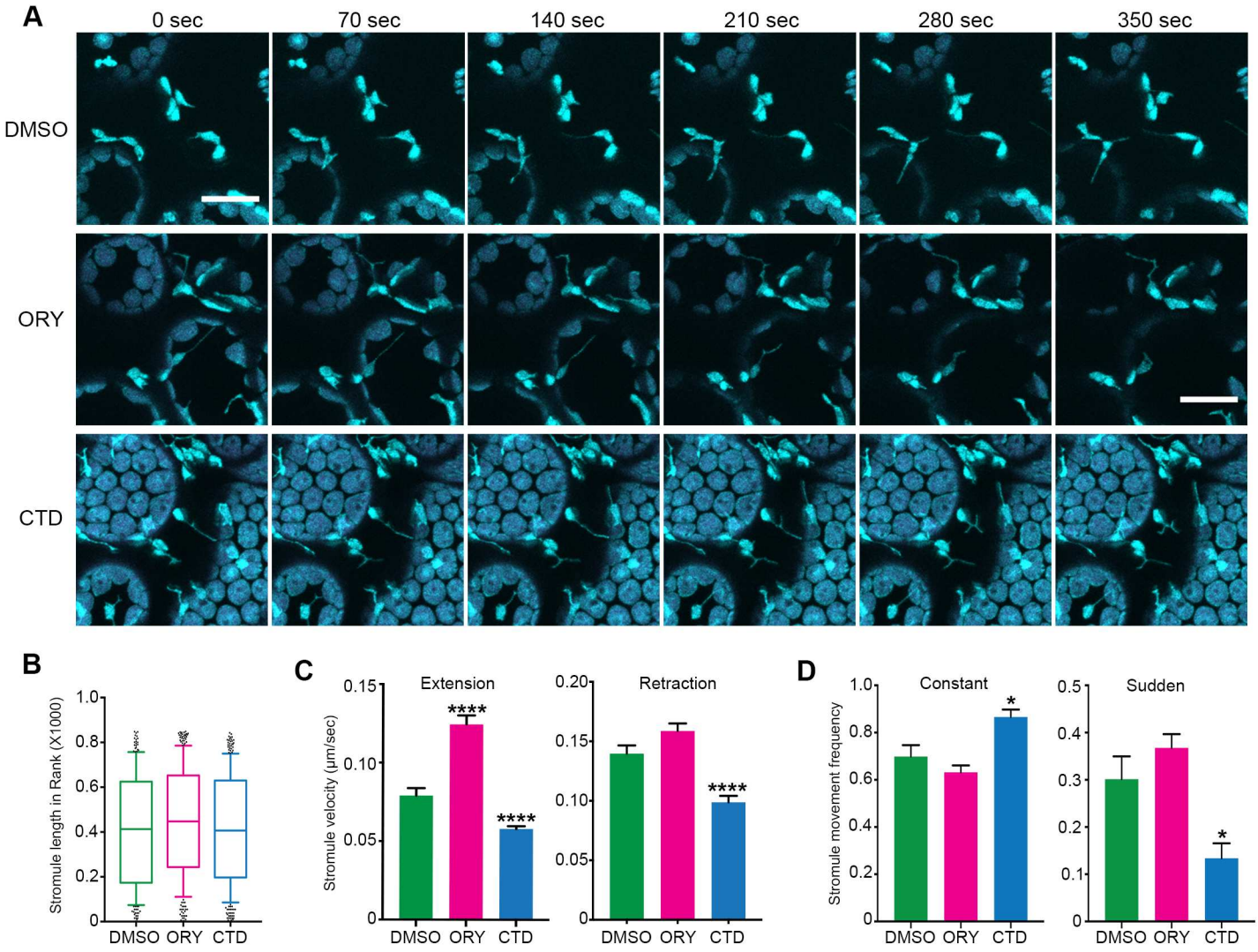
A
0 sec
70 sec
140 sec
210 sec
280 sec
350 sec
DMSO
ORY
CTD
B
Stromule length in Rank (X1000)
1.0
0.8
0.6
0.4
0.2
0
DMSO ORY CTD
C
Stromule velocity (μm/sec)
Extension
0.15
0.10
0.05
0
****
****
DMSO ORY CTD
Retraction
0.20
0.15
0.10
0.05
0
****
DMSO ORY CTD
D
Stromule movement frequency
Constant
1.0
0.8
0.6
0.4
0.2
0
*
DMSO ORY CTD
Sudden
0.5
0.4
0.3
0.2
0.1
0
*
DMSO ORY CTD

Figure 7-figure supplement 1

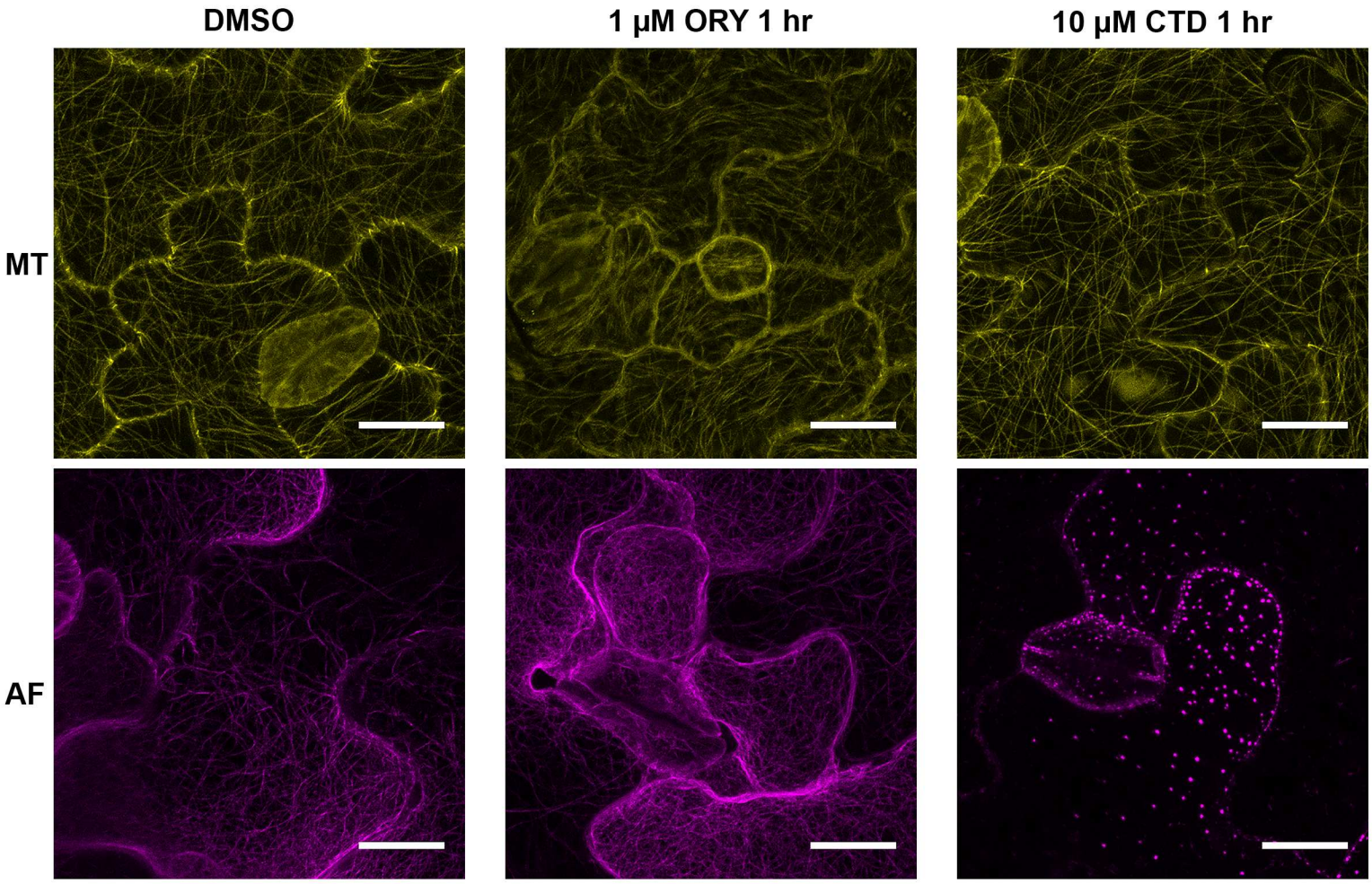

Figure 8

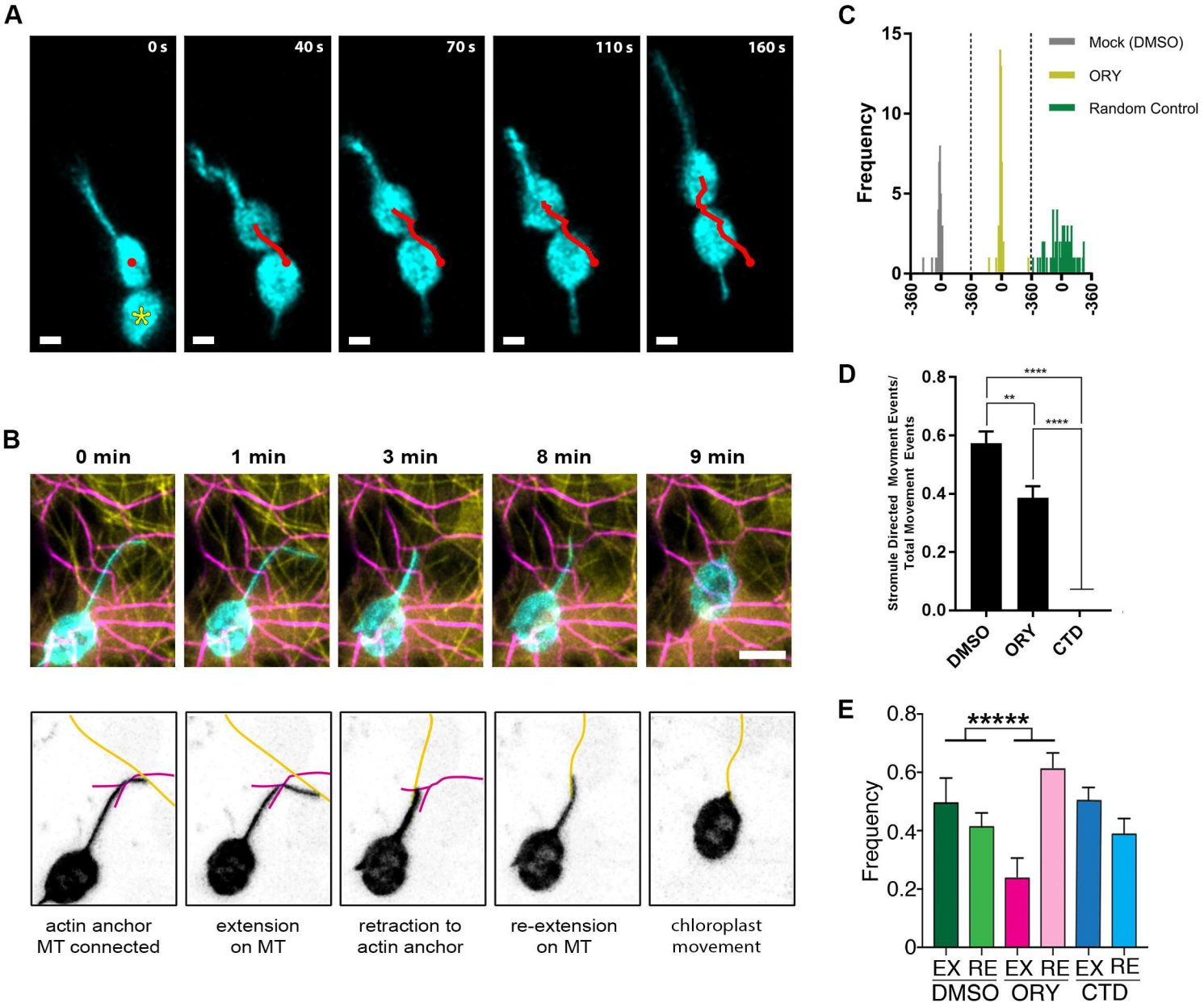
A
0 s
40 s
70 s
110 s
160 s
B
0 min
1 min
3 min
8 min
9 min
actin anchor
MT connected
extension
on MT
retraction to
actin anchor
re-extension
on MT
chloroplast
movement
C
Frequency
Mock (DMSO)
ORY
Random Control
-360
0
D
Stromule Directed Movment Events/
Total Movement Events
DMSO
ORY
CTD
E
Frequency
EX RE
DMSO
EX RE
ORY
EX RE
CTD

Figure 8-figure supplement 1

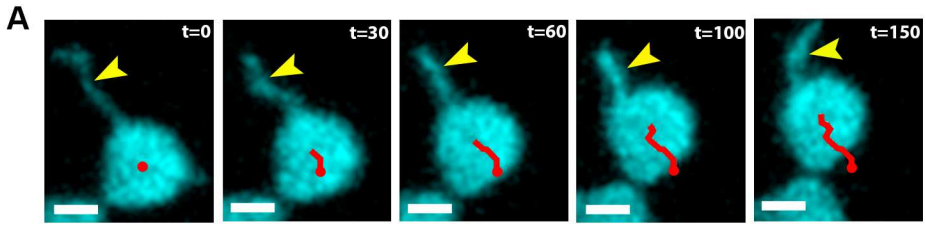

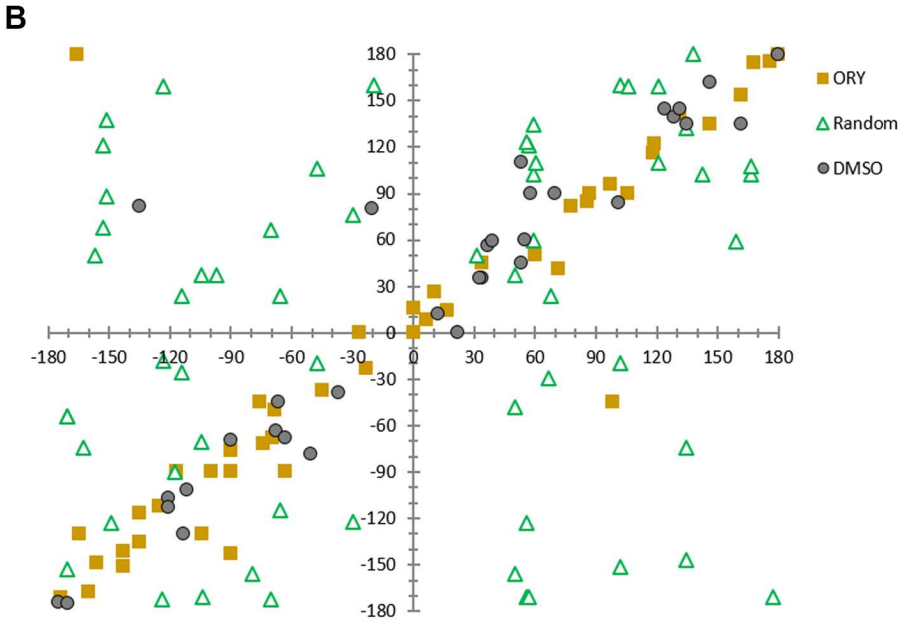

Figure 8- figure supplement 2

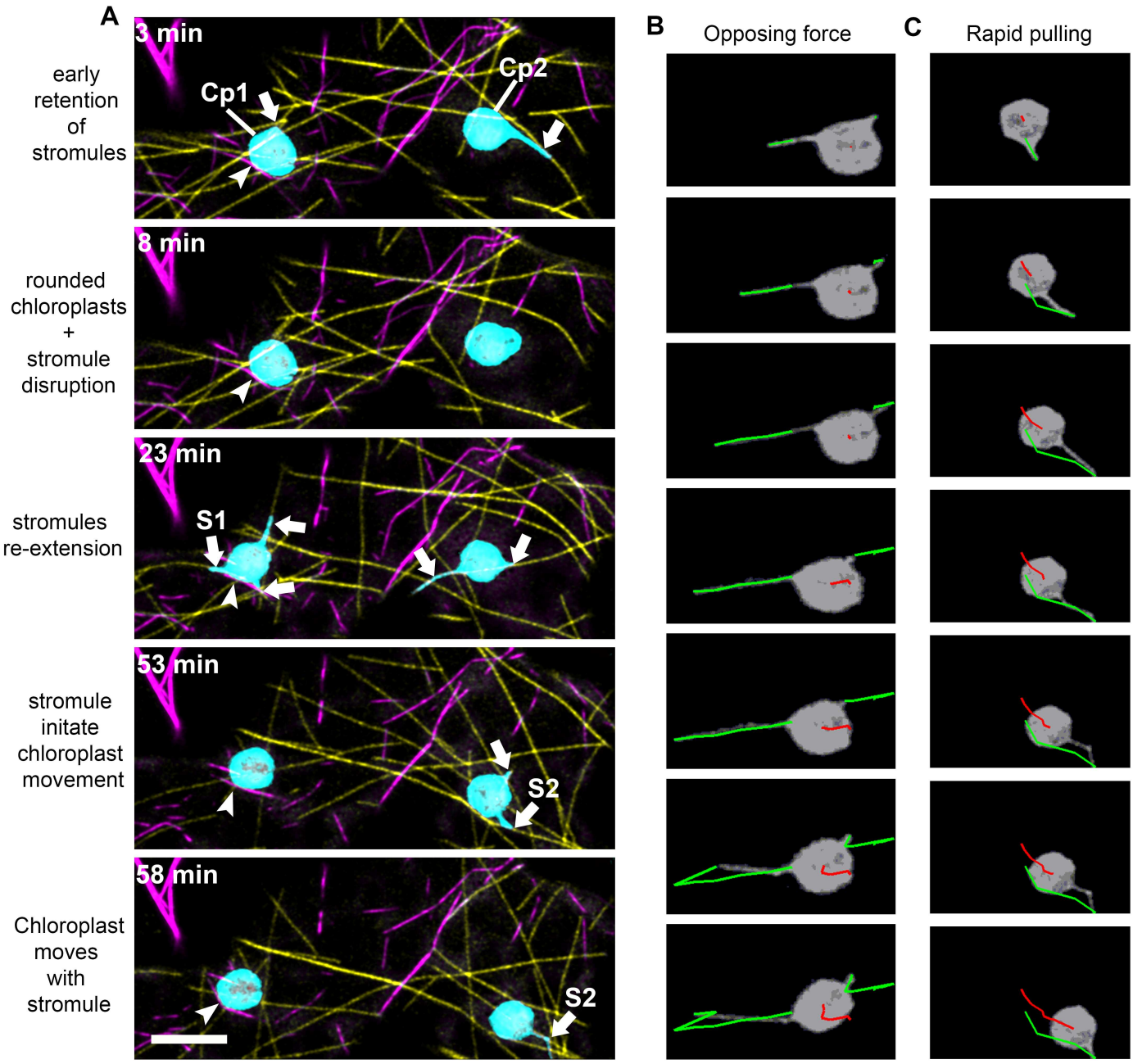

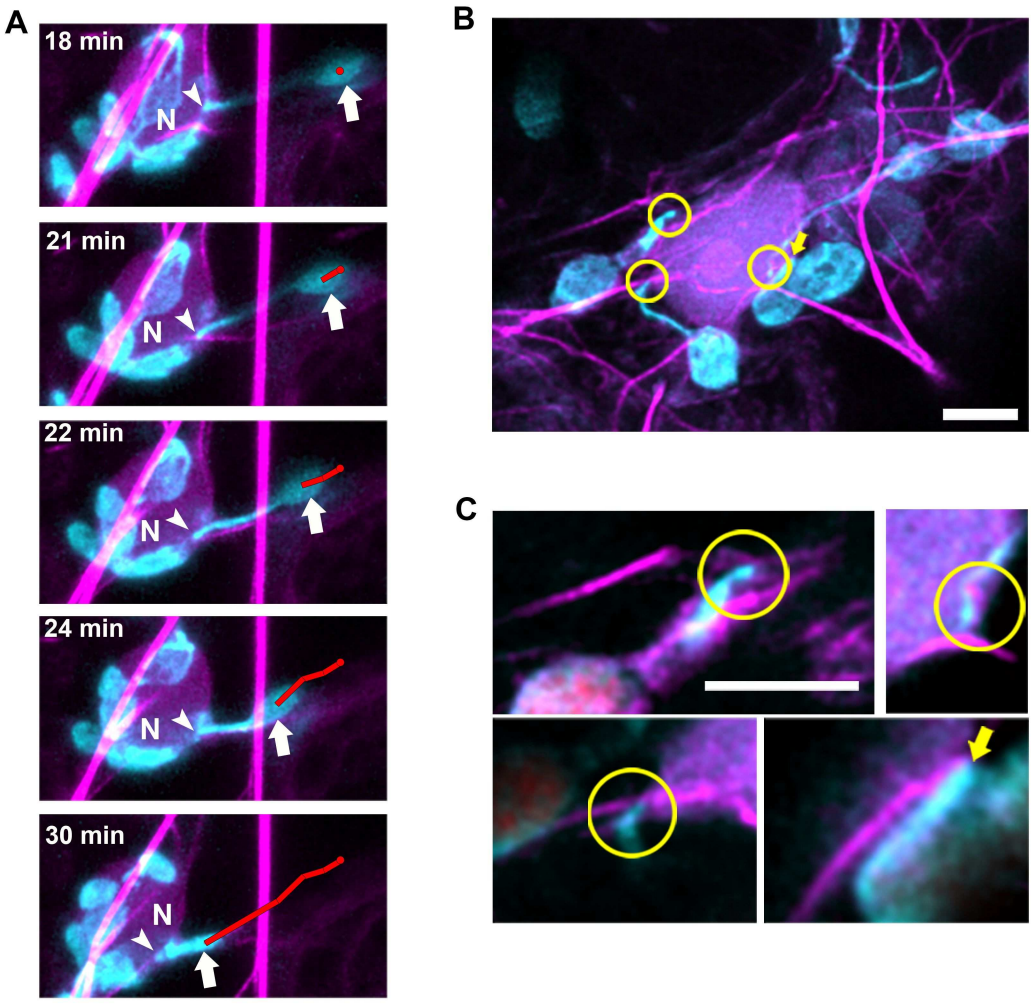
A
18 min
N
21 min
N
22 min
N
24 min
N
30 min
N
B
C

Figure 9-figure supplement 1

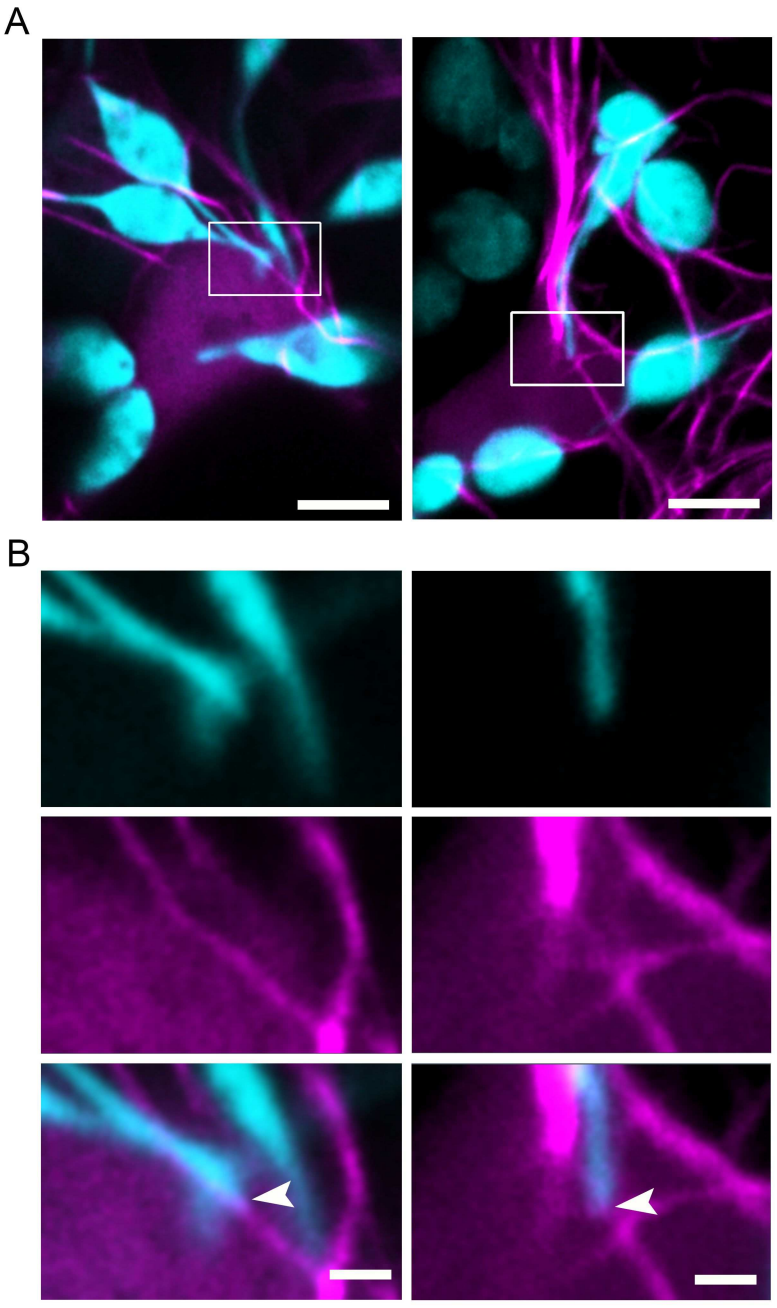

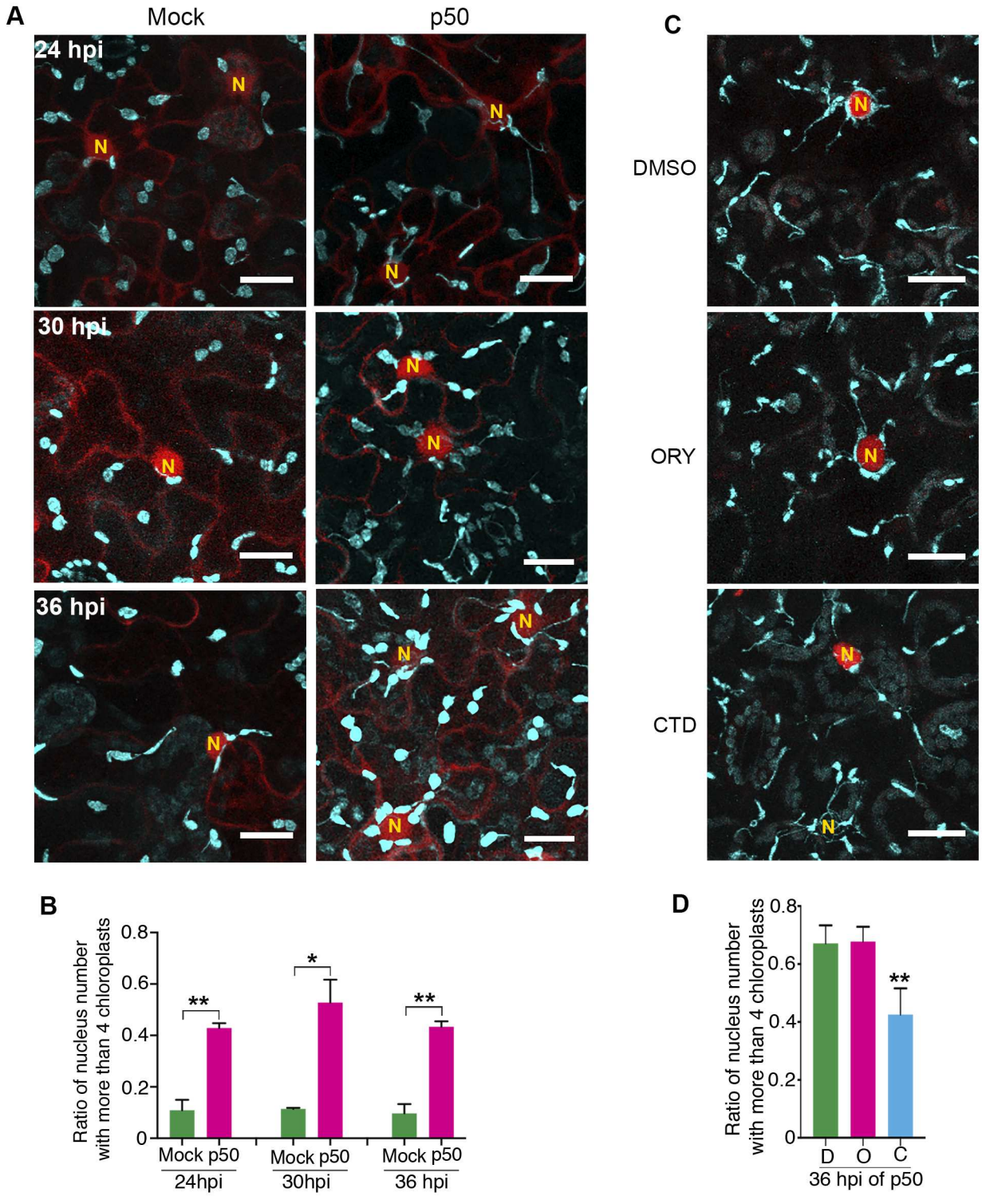
A
Mock
p50
24 hpi
30 hpi
36 hpi
N
C
DMSO
ORY
CTD
B
Ratio of nucleus number with more than 4 chloroplasts
0.8
0.6
0.4
0.2
0
**
*
**
Mock p50
24hpi
Mock p50
30hpi
Mock p50
36 hpi
D
Ratio of nucleus number with more than 4 chloroplasts
0.8
0.6
0.4
0.2
0
**
D
O
C
36 hpi of p50

Figure 10-figure supplement 1